Journal of Archaeological Science: Reports 64 (2025) 105131

Contents lists available at ScienceDirect

Journal of Archaeological Science: Reports

journal homepage: www.elsevier.com/locate/jasrep

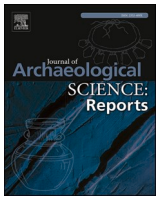

A non-invasive archaeometric protocol for characterizing possible *Corallium rubrum*-related carbonate materials in decorations on Iron Age bronze fibulae of the Golasecca culture

Giulia Berruto [a,*], Eliano Diana [b], Roberto Giustetto [a,c,d]

[a] Department of Earth Sciences, Università di Torino, via Valperga Caluso 35, 10125 Torino, Italy
[b] Department of Chemistry, Università di Torino, via P. Giuria 7, 10125 Torino, Italy
[c] NIS (Nanomaterials for Industry and Sustainability) Centre, via Quarello 11, 10135 Torino, Italy
[d] INFN (National Institute of Nuclear Physics), via Giuria 5, 10125 Torino, Italy

ARTICLE INFO

Keywords:
Golasecca culture
Red coral
Calcite
bronze Iron Age fibula
Whitish decoration

ABSTRACT

In the Iron Age, the Golasecca culture in Northwestern Italy connected Italic populations with transalpine and Celtic ones. From the 7th century BCE, in some jewellery artefacts (bronze fibulae and pendants) a whitish material constituting either part of the objects or nestled decorations is observed. Archaeologists identify it as coral (*Corallium rubrum*), its red hue whitened by the passing of time. However, few archaeometric studies have been carried out so far, also because of their invasiveness. 46 artefacts with whitish decorations from the archaeological sites of Como, Castelletto Ticino and Golasecca (stored in the Museo Civico Archeologico 'P. Giovio', in Como) are investigated here with a novel, non-destructive, multi-analytical protocol (i.e., μ-Raman spectroscopy, μ-X-ray diffraction, optical microscopy and SEM-EDS in low-vacuum), which completely safeguards their integrity. This approach, applied on the artefacts as such, allows identifying their constituent materials and degradation byproducts, extrapolating information about their nature, history and manufacturing process. Ca-carbonates – in the form of calcite – are identified in the decorations of most studied artefacts. This evidence alone does not account for their biologic origin (i.e., from *C. rubrum*), but other aspects can help in solving such an issue. In several artefacts, high-Mg calcite (HMC, a marker for biogenic carbonates) + polyenes (the typical pigments of red coral), sole HMC or even a mixture of HMC + LMC are identified – often coupled to typical coral micro-morphologies. A biogenic origin for these carbonates (i.e. red coral, though other similar species cannot be completely ruled out) can certainly be ascertained – lack of polyenes being justified by possible denaturation over time. In other artefacts, however, low-Mg-calcite (LMC) or even pure-calcite (i.e., with no detectable Mg) are found with no polyenes – hinting a possible inorganic origin. Most of these, however, show typical coral micro-morphologies. In these decorations, Mg-depletion might thus depend on the meteoric diagenesis of originally biogenic carbonates, responsible for transformation of HMC to LMC (or even pure-calcite) and decay of polyenes. Other materials are also seldom detected – i.e., gypsum, probably resulting from sulfation of an original coralline matrix interred in acidic soils, and Ca-phosphates, due to sporadic use of bones. All these evidences point to the fact that *C. rubrum* was feasibly used in at least ≈ 70 % of the studied decorated artefacts. For what concerns the composition of the alloy, bronze or lead-bronze can be found in different artefacts – or even different portions of the same item – possibly depending on sharp technological issues, dictated by fluidity or workability during manufacture.

1. Introduction

Mediterranean red coral (*Corallium rubrum*) is a marine invertebrate with a calcareous skeleton, which fascinated humans since the ancient times (Tagliente, 2006). Coral is found in archaeological contexts as early as the Neolithic (Borrello, 2001; Borrello et al., 2012; Skeates, 1993). In the Iron Age (7th century BCE), it was used in Northern Italy and Europe to produce jewellery and among the Celtic populations as an

* Corresponding author.
E-mail address: giulia.berruto@unito.it (G. Berruto).

https://doi.org/10.1016/j.jasrep.2025.105131
Received 4 October 2024; Received in revised form 28 February 2025; Accepted 3 April 2025
Available online 13 April 2025

exotic material (Ugolini, 2006). Testimonies are found in the Golasecca and Este cultures in the western and eastern regions, respectively (de Marinis, 2000; Mangani, 2016; De Marinis, 1997). In Golasecca, coral was used from the beginning of the 7th century BCE in different artefacts – mainly pendants and bronze fibulae decorated by nestled, circular insets of a white-to reddish paste (de Marinis, 2000; De Marinis, 1997). A strict scientific characterization of these decorations has hardly been achieved and the raw materials provenance still represents an unsolved archaeological issue.

An archaeometric survey was recently carried out with a rigorous – albeit micro-destructive –protocol on Iron Age fibulae from archaeological sites of Northern Italy. This proved that coral skeletons – their red colour whitened in time – constitute most decorations, though other materials were used too (Berruto et al., 2023). However, some artefacts integrity was sacrificed, due to sampling. To avoid this, a novel approach is presented here, aimed at collecting data with a totally non-invasive procedure on the fibulae as such and tested on the collection of the Museo Civico Archeologico 'P. Giovio' in Como (Italy). 46 (out of 62) Northwestern Italy artefacts with preserved decorations were analysed (Peroni et al., 1975; Von Eles Masi, 1986). 45 refer to the Golasecca culture (Fig. 1): 5 from Castelletto Ticino (near Novara, Piedmont; Fig. 2a), 8 from Golasecca (near Varese, Lombardy; Fig. 2b) and 32 from Como (Lombardy; Fig. 2d-e-f). The residual one is from Sampeyre-Mandam (near Cuneo, Piedmont, Fig. 2c; Faudino et al., 2014).

2. Materials and methods

2.1. Archaeological setup

Extending across Lombardy, Piedmont, Canton Ticino and Mesolcina Valley, the Golasecca culture was bordered by the Po, Sesia and Serio/Adda rivers to the south, west and east, respectively. Different facies exist, from the protohistoric Final Bronze Age (Protogolasecca: 900 BCE) to the "Gallic invasions" of Northern Italy (380 BCE) and the La Tène period. Specific ensembles and forms correspond to this culture, divided into three facies split into sub-phases (Table 1; Casini, 2022; Cicolani et al., 2017; De Marinis and Gambari, 2005; Peroni et al., 1975). Evidence is mostly related to funerary contexts, the knowledge of the settlements being scarce (De Marinis, 2009a).

Between the 8th and 7th centuries BCE, the proto-urban pole of Como got in touch with the Bologna and Etruria populations (Casini, 2022). From the 7th century BCE, a change occurred with the rise of the Castelletto Ticino-Sesto Calende-Golasecca pole, which became hegemonic in the trades with the Etruscan and Italic people to the south and transalpine Celts to the north (De Marinis, 2009a; De Marinis, 2009b). In necropolises, sumptuous tombs of warrior princes are related to the GI phase, and become infrequent from the 6th century BCE on. Contacts with the Etruscans became more evident and sumptuous female tombs are attested. From the 5th century BCE on, new settlements emerged and the Castelletto Ticino-Sesto Calende-Golasecca pole lost its importance in favour of Como. The ceramic and metallurgic production became consolidated from the GII to GIIIA phase, along with signs of Etruscan influences, with a development of the Northern areas (Monte Ceneri and the Mesolcina Valley; De Marinis, 2009b).

Fig. 1. Map of the investigated archaeological sites (white stars) with respect to the Golasecca culture area (red circle) in Northwestern Italy (Piedmont and Lombardy regions). (For interpretation of the references to colour in this figure legend, the reader is referred to the web version of this article.)

2.2. Materials

The record consists of 44 (out of 62) artefacts of different types and chronologies, marked by a white-to-reddish pasty material either in the decorations or as a constituent (Fig. 2; Table 2[1]; see Supplementary Material, Table 1S, for the excluded finds). Also, 2 additional fragments, previously identified as coral pieces, are included. The main typology is the bronze *sanguisuga* fibulae with extended foot (30 artefacts), with occhio di dado (2) or circular (28) decorations; among these, some have a massive bronze bow (5) while most have a terracotta core (25). Other types include composite bow fibula (6), Longone al Segrino pendant (6), navicella fibula (Valvaraita type) with occhio di dado decoration (1) and grooming tool with circular decoration (1). Morphology and chronology are as follows:

a. Longone type pendants (e.g., # 4, 7, 39, 45–46: Fig. 2) consist of a T-shaped twisted bronze rod, with a loop holding a small sprig of presumed rough coral. Inserted into necklaces and associated to female burials, they relate to the early GIB-GIC phases (De Marinis, 2000).
b. Composite bow fibulae (e.g., # 35, 37–38, 40–42: Fig. 2) consist of a bronze rod holding materials (e.g., coral), referable to the GIC-GII (the simpler shapes) and GIIIA1 phase (more complex ones include gold ribbons; De Marinis, 2000).
c. *Sanguisuga* fibulae with insets (e.g., # 1–2, 5, 9–10, 12–13, 15–34: Fig. 2) are functional and ornamental objects associated with high status female burials, dated – depending on the holes number and arrangement – from the GIIA-B/GIIB to the GIIIA1 phase (advanced Palestro type). The decorations consist of small circular holes on the bow and foot, filled with a whitish material between two bands of transverse lines.
d. Ornamented bronze objects with inlays involve fibulae, bucket pendants and grooming tools (e.g., # 3, 11, 14, 43–44: Fig. 2) (De Marinis, 2000).

Artefacts from Castelletto Ticino and Golasecca belong to a collection assembled in the 19th century CE by Alfonso Garovaglio, then donated to the Como Museum (Roncoroni, 2005). Those from the Como area are mostly from old excavations, sometimes vaguely recorded (e.g., Como surroundings), pertinent to funerary contexts: mainly from the Ca' Morta necropolis, identified in 1885 during railway works, and then further excavated until Rittatore Vonwiller's operations in the 1950 s (De Marinis, 1981). Findings from Prestino (Como), Via Isonzo-La Pesa, come from preventive stratigraphic excavations (1981–85) that

[1] For the archaeological sites located in the Como area, the previous territorial allocation is also shown, now surpassed due to the gathering of several municipalities: Camerlate and Monte Olimpino are gathered with Como since 1884, Rebbio since 1937, Breccia, Albate, Brunate, Civiglio and Camnago Volta since 1943 (De Marinis, 1981).

(caption on next page)

Fig. 2. The studied archaeological artefacts from: a) Castelletto Ticino (NO) [inv. No.: 1) D2073; 2) D2773; 3) D2077; 4) D1750; 5) D2104]; b) Golasecca (VA) [6) D1669; 7) D1668; 8) D1667; 9) D2065; 10) D2049; 11) D1660; 12) D2064; 13) D2059]; c) Sampeyre (CN) [14) E17738]; d) Como (CO), bronze fibulae with circular decoration, from funerary context [inv. No.: 15) St114084; 16) St114083; 17) St2208; 18) St2206; 19) E13225; 20) E5873; 21) St139651; 22) St139652; 23) St879; 24) E5868; 25) E5667; 26) E5553; 27) E5865; 28) E5552]; e) Como (CO), bronze fibulae with circular decoration, from settlement context [inv. No.: 29) St57216; 30) St57220; 31) St57210; 32) St57244; 33) St57262; 34) St57250]; f) Como (CO), other typologies [inv. No.: 35) St1993; 36) St124133; 37) St1397; 38) E13273; 39) St124142; 40) St1230; 41) E5957; 42) E5958; 43) St864; 44) St865; 45) St33594; 46) St33593].

Table 1
Chronological partitioning of the Golasecca culture.

Phase	Sub-phases	Chronology
Golasecca I (GI)	GIA1	900–825 BCE
	GIA2	825–750 BCE
	GIB	750–675 BCE
	GIC	675–620 BCE
Golasecca II (GII)	GIIA	620–575 BCE
	GIIA/B	575–520 BCE
	GIIB	520–480 BCE
Golasecca IIIA (GIIIA)	GIIIA1	480–450 BCE
	GIIIA2	450–420 BCE
	GIIIA3	420–380 BCE

discovered residential structures and drainage canals, artificial fillings and metalworking; 6 artefacts were found in a crucible for remelting (Casini, 2018, 2022). Most finds (29) show no sign of combustion, though eight underwent an evident burning (Table 2). Combustion is an important issue, since polyenes – the red coral chromophore pigments – become volatile at ≈ 200 °C (Bente et al., 2015). However, the identification of an intervened combustion is not always straightforward based on surface examination. For some finds lacking traces of combustion, the context of the finding (e.g., a crucible) may suggest that this event may have occurred (Casini, 2018).

The whitish decorating materials are defined in the archaeological literature as *C. rubrum* whitened in time (De Marinis, 2000; Perrin, 2000), but archaeometric validations are few (Angelini and Molin, 2015; Mangani, 2016). Red coral was first used in the GI phase in the form of branches, while from the GII phase on, as a covering element either of the fibula bow or as a decoration of the fibula itself (Berruto et al., 2023; De Marinis, 2000). The skeleton of *C. rubrum* is mainly made of Ca-carbonate in the form of calcite ($CaCO_3$), with a minor Mg^{2+} content and few other trace elements. In biogenic calcite (such as coral), $MgCO_3$ occurs in the 9-to-15 mol % range (high magnesian calcite: HMC). In fresh red coral skeletons, the hue is provided by a mixture of partially/completely demethylated polyenes, whose chemistry is still debated, gradually denaturing in time (Barnard and de Waal, 2006; Bergamonti et al., 2011, 2013; Brambilla et al., 2012; Fernandes et al., 2015; Fürst et al., 2016; Hasegawa et al., 2012; Kaczorowska et al., 2003; Kiefert and Karampelas, 2011; Kupka et al., 2009; Macchia et al., 2016; Maia et al., 2010; Rahman et al., 2011; Smith et al., 2007; Vielzeuf et al., 2008, 2013).

2.3. Methods

A multi-analytical approach is needed to efficiently characterize these decorative materials (Angelini and Molin, 2015; Bente et al., 2015; Berruto et al., 2023; Fürst et al., 2016; Giustetto et al., 2013; Mangani, 2016; Schrickel et al., 2013; Schvoerer et al., 2000). Unfortunately, this approach is often micro-destructive, requiring the extraction of micro-samples and undermining the artefacts integrity. The need for a non-invasive protocol, capable of identifying *C. rubrum* (or any other material) without endangering the artefacts, is thus required. This approach is tested here for the first time and includes – in addition to the standard archaeological and photographic documentation – optical microscopy, micro-Raman spectroscopy, micro-X-ray diffraction (μ-XRD) and scanning electron microscopy with energy-dispersive spectrometry (SEM-EDS).[2]

Optical microscopy (OM) was performed at first in the museum, selecting the artefacts with presumed coral, and then in the laboratory, observing their details, preservation conditions and extrapolating information about their origin and production technology. A MAOZUA 5MP 20-300x digital microscope was used in the first instance; a OPTIKA SZO-4 stereomicroscope, equipped with a OPTIKA C-B18 + camera in the following.

μ-Raman spectroscopy was used to detect organic/inorganic compounds and identify the pigments of *C. rubrum*. Data were collected with a Horiba Jobin Yvon HR800 spectrometer, with polarized green laser (solid state Nd; wavelength 532 nm; power 250 mW) and edge filter, 600 grooves/mm gratings, an air-cooled CCD detector equipped with an Olympus BX41 optical polarizing microscope. 10X/20X magnifications and filters (between 0.6 and 2) in the 100–2000/4000 cm^{-1} spectral range (2 acquisitions, 6 s each) were used. Si was used to calibrate the spectrometer. The Labspec 5 software was adopted for imaging and data collection and the OPUS 6.0 software for data interpretation, by comparing the experimental signals with the RRUFF™ Project database (Lafuente et al., 2015).

μ-XRD enables identification of crystalline phases and was performed on a SMARTLAB XE – Rigaku diffractometer in μ-diffraction mode and a zero-background, Si mono-crystal flat sample holder, in the 3/70° 2θ range with mono-chromatized Cu-Kα radiation. Experimental parameters: Detector: HyPix-3000 (vertical); Scan mode: 1D (scan); Energy mode: standard; Slit: 2 mm; Step-increment: 0.02°; Speed: 0.5°/min. Data were interpreted with the 'DIFFRAC PLUS, EVA 7.0.0.1′ software (2001), by comparing the positions and intensities of the reflections with the JCPDS-ICCD, ICSD and PCPDFWIN databases.

SEM in low vacuum allows observing at high-magnification the artefacts surface, and EDS allows collecting semi-quantitative chemical analyses. The method is used for quantifying the Ca/Mg ratio in the carbonate – suitable for discriminating its biotic/abiotic nature and identifying the organism responsible for its production (e.g., *C. rubrum* or *Spondylus gaederopus*, whose skeleton/shell contains both calcite and polyenes; Berruto et al., 2023; Fürst et al., 2016). A JEOL JSM IT300LV SEM was used (High Vacuum – Low Vacuum 10/650 Pa – 0.3–30 kV) coupled with an EDS Oxford INCA Energy 200 equipped with an X-act SDD thin window detector, for analysis of light elements (down to B). Data were collected in low vacuum (35 Pa) on uncoated samples. Standardization was performed using pure Co. Working parameters: acceleration voltage 15 kV; working distance 10–13 mm; probe current 1nA; spectra acquisition time varying from 60 to 300 s. The Inca 200 Microanalysis Suite Software (version 4.08) was used for data collection/elaboration.

3. Results

A detailed compositional analysis of both decorations and metal alloy was performed for each artefact. The related outcomes are detailed

[2] Application of the analytical protocol needed the artefacts to be moved from the 'P. Giovio' museum to the scientific laboratories and then brought back. This was done in accordance with due authorisations obtained by the 'Soprintendenza Archeologia Belle Arti e Paesaggio per le province di Como, Lecco, Monza Brianza, Pavia, Sondrio e Varese' (prot. 5174 dated 01/03/2022) and the Municipality of Como (prot. 23307 dated 01/04/2022).

Table 2
Investigated archaeological finds [Abbreviations: T. = tombs; Rest. = restored] – type abbreviations: 1) Sanguisuga fibula with terracotta core and circular insets; 2) Sanguisuga fibula with full-bow and circular insets; 3) Sanguisuga fibula with terracotta core and occhio di dado decoration; 4) Composite bow fibula; 5) Longone al Segrino pendant; 6) Sanguisuga fibula's foot with circular insets; 7) Valvaraita fibula; 8) grooming tool; 9) little element].

Inv. no.	Site	Discovery	Chronology	Phase	Type	Burnt	Rest.
St864; E3254	Como, Ca' Morta, Rebbio, Cava Manzoni, T.2	1926	6th c. BCE	GII	3	NO	NO
St865; E3255	Como, Ca' Morta, Rebbio, Cava Manzoni, T.2	1926	6th c. BCE	GII	3	NO	NO
St879; E3269	Como, Ca' Morta, Rebbio, Cava Ballerini, T.VI	1926	550–480 BCE	GIIA-B	1	NO	NO
St1230; E3620	Como, Ca' Morta, Rebbio, loc. Ronchetti, Fondo Porciani e Cattaneo, T.?	1953	480–440 BCE	GIIIA	4	NO	YES
St1397; E3787	Como, Ca' Morta, Cava Butti, T.116	1959	480–440 BCE	GIIIA	4	NO	NO
St1993; E4022	Como, Ca' Morta, Rebbio, T.131	1959	675–600 BCE	final GIB	4	?	NO
St2206; E4385	Como, Ca' Morta, Cava dalla Zuanna, T.177centr.	1963	525–480 BCE	GIIB	2	NO	YES
St2208; E4387	Como, Ca' Morta, Cava dalla Zuanna, T.177centr.	1963	525–480 BCE	GIIB	2	NO	YES
St33593; E5271	Como, Ca' Morta, terreno IACP a nord di via Cecilio, T.302	1979	7th c. BCE	final GIB	5	NO	YES
St33594; E5272	Como, Ca' Morta, terreno IACP a nord di via Cecilio, T.302	1979	7th c. BCE	final GIB	5	NO	YES
St57210	Como, Prestino, via Isonzo	1981	475–410 BCE	GIIIA	1	YES?	YES
St57216	Como, Prestino, via Isonzo	1981	475–410 BCE	GIIIA	1	YES?	YES
St57220	Como, Prestino, via Isonzo	1981	475–410 BCE	GIIIA	1	YES?	YES
St57244	Como, Prestino, via Isonzo	1981	475–410 BCE	GIIIA	1	YES?	YES
St57250	Como, Prestino, via Isonzo	1981	475–410 BCE	GIIIA	1	YES?	YES
St57262	Como, Prestino, via Isonzo	1981	475–410 BCE	GIIIA	1	YES?	YES
St114083; E5384	Como, Ca' Morta, Rebbio, T.238	1969	550–525 BCE	GIIA-B	2	NO	YES
St114084; E5385	Como, Ca' Morta, Rebbio, T.238	1969	550–525 BCE	GIIA-B	2	YES	YES
St124133; E4537	Como, Ca' Morta, Rebbio, T.197	?	6th-5th c. BCE	GII	9	YES	NO
St124142; E4491	Como, Ca' Morta, Rebbio, Cava Bianchi, T.200	1950–1970?	750–675 BCE		5	NO	NO
St139651; E4932	Como, Ca' Morta, Rebbio, T.256	1975	525–480 BCE	GIIB	1	NO	NO
St139652; E4933	Como, Ca' Morta, Rebbio, T.256	1975	525–480 BCE	GIIB	1	NO	NO
E5552	Como, dintorni	pre-1892	480–410 BCE	GIIIA	1	NO	NO
E5553	Como, dintorni	pre-1892	480–410 BCE	GIIIA	1	NO	NO
E5667	Como, dintorni	pre-1892	525–480 BCE	GIIB	1	NO	YES(?)
E5865	Como, Ca' Morta, Rondineto, proprietà Galli	pre-1892	480–410 BCE	GIIIA	1	NO	YES
E5868	Como, Ca' Morta, Rondineto	pre-1892	600–480 BCE		1	NO	YES
E5873	Como, Ca' Morta, Rondineto	pre-1892	550–440 BCE	GIIA-B	6	NO	YES
E5957	Como, Respaù, Monte Olimpino	1800?	475–410 BCE	GIIIA	4	NO	YES
E5958	Como, Respaù, Monte Olimpino	1800?	475–410 BCE	GIIIA	4	NO	YES
E13225	Como, Rebbio, Villa Giovio	1927	480–440 BCE	GIIIA	6	?	NO
E13273	Como, Ca' Morta	1800?	7th-5th c. BCE	GI-GII	4	?	NO
E17738	Val Varaita, Sampeyre-Mandam	1800?	480–425 BCE.	NO	7	NO	YES
D1660	Golasecca	1800?	end of 6th-5th c. BCE		8	YES	NO
D1667	Golasecca	1800?	?		9	YES	NO
D1668	Golasecca	1800?	7th c. BCE	final GIB	5	NO	YES
D1669	Golasecca	1800?	7th c. BCE	final GIB	5	YES	YES(?)
D1750	Castelletto Ticino	1878	end of 8th-7th c. BCE	GIB-C	5	NO	NO
D2049	Golasecca	1800?	525–480 BCE	GIIB	1	NO	NO
D2059	Golasecca	1800?	525–480 BCE	GIIB	1	NO	YES
D2064	Golasecca	1800?	6th c. BCE	GII	1	YES	YES
D2065	Golasecca	1800?	6th c. BCE	GII	1	YES	NO
D2073	Castelletto Ticino	1800?	560–525 BCE	GIIA-B	1	YES	NO
D2077	Castelletto Ticino	1878	560–525 BCE	GIIA-B	2	NO	NO
D2104	Castelletto Ticino	1878	560–525 BCE	GIIA-B	1	NO	YES
D2773	Castelletto Ticino	1877	560–525 BCE	GIIA-B	1	NO	YES

in Table 3 and 4, respectively.

3.1. *Decorating materials*

Calcite is detected in most artefacts – often traceable to coral and in some cases with a more questionable origin. However, different materials are also sporadically observed. In 11 artefacts (≈ 24 % of the studied record), no trace of decorating material is found, but only soil residues and bronze alteration byproducts (Fig. 3).

3.1.1. *Coral-related carbonate materials*

In 7 artefacts (St57210/216/220/244/250/262 and E13225, all *sanguisuga* fibulae with circular insets from Como, via Isonzo – Fig. 2, # 31, 29, 30, 32, 34, 33 and 19 – found in a crucible and dated to GIIIA – 475–410 BCE; Table 3) HMC is identified together with polyenes. The former is detected by μ-XRD (together with azurite, malachite, cuprite and cerussite, related to bronze alteration byproducts) and SEM-EDS, with an average content of ≈ 14.80 $MgCO_3$ mol % (ranging from 2.55 to 19.99 %). Relevant amounts of Na and S support the biogenic nature in marine environment of these carbonates, whereas traces of other elements (i.e., Al, Si, Cl, K, Fe, Cu, Ag, Sn, Pb) could be related to soil residues and alloy alteration (Fig. 4). Polyenes are detected by μ-Raman (bands at 1518/1521 and 1134 cm^{-1}) together with calcite only in these seven artefacts, certifying – despite their finding context (i.e., in a crucible) – that they underwent no combustion (which would have caused these pigments to decay). Typical coral micro-morphologies (e.g., garland-like) are also observed at the optical microscope (Fig. 5c). Beeswax is detected by Raman (bands at 2883 and 2846 cm^{-1}: Fig. 6) only in one case (St57244; Fig. 2, # 32).

In 5 other artefacts (E5868/957/958; D1750/2077, two *sanguisuga* fibulae, two composite bow fibulae and a Longone pendant, with no evident signs of burning and variable chronology – Fig. 2, # 24, 41, 42, 4_and 3; Table 3), HMC is found by both μ-XRD (with quartz, albite, anorthite and possibly teallite as subordinate phases) and SEM-EDS (average Mg content ≈ 15.26 $MgCO_3$ mol %, ranging from 5.87 to 28.43; Table 3), but Raman finds no polyenes. For these specimens, only calcite is detected by μ-Raman (whose bands are shifted at higher wavenumbers – from 1089 to 1092 cm^{-1} – supporting the high Mg-content: Borromeo et al., 2017). In spite of this, some of the typical micro-features of coral (i.e., longitudinal crenulations of gastrodermal canals – in E5957, E5958 and D1750; Fig. 2, # 41, 42 and 4 – or wavy concentric growth rings in the annular region – in D1750; Fig. 5a-b) are

Table 3
Mineralogical and chemical information inferred by the adopted totally-non-invasive archaeometric protocol on the white parts of the 46 investigated archaeological finds [Interpr. = interpretation; NO = not executed].

Artefact	μ-Raman	μ-XRD	SEM-EDS in low-vacuum	Attribution
St864; E3254	quartz	NO	Cu + Al, Si + Mg, P, S, Ca, Fe, Sn	No dec.
St865; E3255	–	quartz	Al, Si, Cu, Sn + Na, Mg, S, K, Ca, Ti, Fe, Pb	No dec.
St879; E3269	calcite 1088	calcite, albite, anorthite	LMC 3,68 % Mg (3,40–3,97 %) Ca + Mg, Al, Si, P, S, Cu	LMC
St1230; E3620	calcite 1090	calcite, albite, anorthite	LMC 5,55 % Mg (0–8,89 %) Ca + Na, Mg, Al, Si, P, S, Cl, K, Ti, Fe, Cu	LMC
St1397; E3787	calcite 1088	calcite, albite, anorthite	LMC 3,69 % Mg (1,28–9,61 %) Ca + Mg, Al, SI, S, K, Fe, Cu	LMC
St1993; E4022	apatite	whitlockite	P, Ca + Na, Mg, Al, Si, S, Cl, K, Ti, Fe, Cu, Sn	Bone
St2206; E4385	calcite 1089, quartz	calcite Mg, malachite, quartz	LMC 3,99 % Mg (1,67–14,86 %) Ca + Na, Mg, Al, Si, P, S, Cl, K, Ti, Fe, Cu, Sn	HMC-LMC
St2208; E4387	quartz?	NO	Cu + Mg, Al, Si, S, Ag	No dec.
St33593; E5271	gypsum	gypsum	S, Ca + Mg, Al, Si, Cl, K, Fe, Cu	Gypsum
St33594; E5272	calcite 1089	calcite, quartz, albite, anorthite, gypsum?, portlandite?	Cu + Si, S, Ca + Mg, Al, P, Cl, K, Mn, Fe, Sn	Calcite
St57210	calcite 1089 + polyenes	calcite Mg, pyromorphite	HMC 13,64 % Mg (11,31–1511 %) Ca + Na, Mg, Al, Si, P, S, Cl, K, Fe, Cu, Ag, Sn, Pb	*C. rubrum*
St57216	calcite 1089 + polyenes	calcite Mg, albite, anorthite	HMC 12,7% Mg (4,85–18,3%) Ca + Mg, Al, Si, P, S, Cl, K, Fe, Cu, Pb	*C. rubrum*
St57220	calcite 1083 + polyenes	calcite Mg	HMC 17,84 % Mg (16,25–19,65 %) Ca + Mg, Al, Si, P, S, Cl, Fe, Cu, Sn, Pb	*C. rubrum*
St57244	calcite 1086 + polyenes + beeswax	quartz, azurite, malachite, cerussite	Cu + Na, Mg, Al, Si, P, S, Cl, K, Ca, Fe, Pb	*C. rubrum*
St57250	calcite 1089 + polyenes	calcite Mg, azurite, cuprite	HMC 11,0% Mg (2,55–16,30 %) Ca + Mg, Si + Na, Al, P, S, Fe, Cu, Pb	*C. rubrum*
St57262	calcite 1089 + polyenes	calcite Mg, cerussite, malachite, azurite, quartz, pyromorphite	HMC 18,81 % Mg (17,17–19,99 %) Ca + Na, Mg, Al, Si, P, S, Cl, K, Fe, Cu, Sn, Pb	*C. rubrum*
St114083; E5384	calcite 1088	NO	LMC 1,53 % Mg (0–4,6%) Ca + Mg, Si, Cu, Sn	LMC
St114084; E5385	calcite 1087	NO	Ca + Si, Cu	Calcite
St124133; E4537	apatite?	Carbonate hydroxyapatite	P, Ca + Na, Mg, Al, Si, S, K, Fe	Bone
St124142; E4491	calcite 1089 + apatite?	calcite, quartz, albite, anorthite	LMC 4,9% Mg (2,52–7,77 %) Ca + Na, Mg, Al, Si, P, S, Cl, K, Fe, Cu	LMC
St139651; E4932	calcite 1089	calcite, malachite, quartz, albite, anorthite	LMC 4,54 % Mg (2,31–6,84 %) Ca + Mg, Al, Si, Fe, Cu	LMC
St139652; E4933	calcite 1087	malachite, quartz	Si + Al, Cu + Mg, P, S, K, Ca, Ti, Fe	No dec.
E5552	–	quartz, dolomite	Cu, Si + Mg, Al, P, S, Cl, K, Ca, Fe, As, Sn	No dec.
E5553	–	quartz, cerussite, malachite	Si + Mg, Al, S, K, Ca, Fe, Cu	No dec.
E5667	–	quartz, albite, anorthite, dolomite	Si, Cu + Mg, Al, S, Cl, K, Ca, Fe	No dec.
E5865	–	NO	Si, Cu + Mg, Al, P, Cl, K, Ca, Fe	No dec.
E5868	calcite 1089	calcite Mg, quartz	HMC 16,1% Mg (11,5–19,9%) Ca + Na, Mg, Al, Si, P, S, Cl, K, Fe, Cu, Sn, Pb	HMC
E5873	–	–	Cu, Sn, Pb + Al, Si, P, Fe	No dec.
E5957	calcite 1089	calcite Mg, albite, anorthite, teallite, silver?, mckinstryte?	HMC 14,09 % Mg (5,87–29,77) Ca + Na, Mg, Al, Si, P, S, Cl, K, Fe, Cu, Ag	HMC
E5958	calcite 1090	calcite Mg, albite, anorthite, teallite?	HMC 19,57 % (12,24–28,43 %) Ca + Mg, Al, SI, P, S, Cl, K, Fe, Cu, Ag	HMC
E13225	calcite 1089 + polyenes	quartz, cerussite	Si, Cu + Mg, Al, S, K, Ca, Fe, Pb	*C. rubrum*
E13273	calcite 1089	calcite, teallite?. Albite, anorthite, quartz	LMC 3,22 % Mg (0–13,21 %) Ca + Si, Cu + Mg, Al, P. S, Fe	LMC
E17738	–	quartz, albite, anorthite, cuprite	Si + Mg, Al, P, S, K, Ca, TI, Fe, Cu, Sn, Pb	No dec.
D1660	calcite 1089	calcite, cassiterite, malachite	LMC 4,96 %Mg (3,92–5,70 %) Ca, Mg + Al, Si, P, S, K, Cu	LMC
D1667	apatite?	NO	Ca, P + Na, Mg, Al, Si, S, Cl, K, Fe, Cu	Bone
D1668	calcite 1089	calcite, anorthite, albite	LMC 4,25 % Mg (0–8,5%Mg) Ca + Mg, Al, SI, S, Cl	LMC
D1669	calcite 1087	calcite, quartz, albite, anorthite	LMC 2,39 % Mg (0–4,78 %) Ca + Mg, Si, P, S, K, Fe	LMC
D1750	calcite 1092	calcite Mg, quartz	HMC 11,27 % (9,33–13,02 % Mg) Ca + Mg, Al, Si, K, Fe	HMC
D2049	calcite 1086	calcite, albite, anorthite, malachite, cassiterite,	LMC 5,33 %Mg (0–11,26 %) Ca + Mg, Al, Si, P,	LMC

(*continued on next page*)

Table 3 (*continued*)

Artefact	μ-Raman	μ-XRD	SEM-EDS in low-vacuum	Attribution
		tenorite, teallite, tennantite	S, K, Ti, Fe, Cu, Sn, Pb	
D2059	–	calcite, cuprite, paratacamite, malachite, mcguinnessite?	Ca + Al, SI, P, Cu, Pb	Calcite?
D2064	calcite 1090	calcite, cassiterite, tenorite	Si, Ca, Cu + Mg, Al, P, S, Pb	Calcite?
D2065	calcite 1089, anhydrite	gypsum	LMC 6,89 %Mg (4,63–9,15 %) Ca + Mg, Al, Si, S, K, Fe, Cu	LMC + gypsum?
D2073	calcite 1086	calcite, tennantite	Si, Ca, Cu + Mg, Al, P, K, Mn, Fe, Sn, Pb	Calcite?
D2077	–	calcite Mg, albite, anorthite, teallite, butlerite?	NO	HMC
D2104	calcite 1090 + Paraloid/ resin	calcite, albite, anorthite	LMC-HMC 8,5% Mg (4,4–20,4% Mg) Ca, Cu + Mg, Al, Si, P, S, Cl, K, Fe, As, Sn, Pb	HMC-LMC
D2773	–	malachite	Si, Cu + Mg, Al, S, Cl, K, Ca, Fe, Zn, Sn	No dec.

observed at the optical microscope (Fürst et al., 2016; Vielzeuf et al., 2008).

For 2 artefacts (D2104 and St2206, GII phase *sanguisuga* fibulae, unburnt; Fig. 2, # 5 and 18) the situation is even more puzzling, as in different areas of the decorations both HMC and LMC are detected by EDS, with a highly variable rate (1.67 to 20.4 $MgCO_3$ mol %). When averaged, the global Mg-content appears to be rather low (≈ 6.25 $MgCO_3$ mol %) – i.e., below the 9 % threshold fixed for HMC (Bergamonti et al., 2011, 2013; Berruto et al., 2023; Fürst et al., 2016; Hasegawa et al., 2012; Rahman et al., 2011; Vielzeuf et al., 2008, 2013). Neither μ-Raman (no shift of the 1090 cm^{-1} band) nor μ-XRD can help in untying the knot, but observations at the optical microscope – in spite of the severe alteration that affects both the whitish material and the metal alloy – allow recognizing typical garland-like morphologies (Fig. 5d, showing an inset of the St2206 artefact; Fig. 2, # 18;).

In 11 artefacts (St879/1230/1397/114083/124142/139651, E13273, D1660/1668/1669/2049: Fig. 2, # 23, 40, 37, 16,_39, 21, 38, 11, 7, 6 and 10) of various types and chronology (four *sanguisuga* and three composite bow fibulae, three Longone pendants and a grooming tool, two of which with signs of combustion; Table 3) LMC is found by EDS (averaged value ≈ 5.33 $MgCO_3$ mol %; hardly exceeding 9 %). μ-XRD also detects soil components after interment (e.g., plagioclase and quartz) and bronze alteration byproducts (malachite, cassiterite, tenorite, teallite and tennantite). In most of these finds (7 out of 11 ≈ 64 %), typical coral crenulations or garland-like morphologies are observed at the optical microscope.

Finally, pure calcite (with no appreciable Mg-content) is identified by SEM-EDS, μ-XRD and μ-Raman in 5 artefacts (St33594/114084; D2059/2064/2073: Fig. 2, # 45, 15, 13, 12 and 1; three *sanguisuga* fibulae with terracotta core and circular decorations, one with full arch and circular decorations and a Longone pendant; Table 3), together with soil components and bronze alteration byproducts. Occasionally, coral micro-morphologies are observed at the optical microscope (e.g., crenulations in St33594).

3.1.2. Materials other than calcite

Gypsum ($CaSO_4 \cdot 2H_2O$) is identified in two artefacts – the unburnt

Table 4
Mineralogical and chemical information inferred by the adopted totally-non-invasive archaeometric protocol on the bronze alteration products on the 46 investigated archaeological finds [Interpr. = interpretation; NO = not executed].

Inv. no.	μ-Raman	μ-XRD	SEM-EDS	Interpr.
St864; E3254	–	NO	Cu, Sn + Mg, Al, Si, P, S, Fe	bronze
St865; E3255	–	quartz	Cu, Sn + Pb + Mg, Al, Si, P, S, Ca, Cr, Fe, As	Pb bronze
St879; E3269	–	calcite, albite, anorthite	body: Cu + Si + Mg, Al, P, S, Ca, Fe, Sn. Foot: Cu, Sn + Mg, Al, SI, P, S, Cl, K, Ca, Ti Fe, As, Pb. Pin: Cu, Sn + Mg, Al, Si, P, S, Cl, K, Ca, Cr, Fe.	Pb bronze
St1230; E3620	cuprite	calcite, albite, anorthite	Cu + Mg, Al, Si, P, S, Cl, Ca, Fe, Sn	Bronze
St1397; E3787	–	calcite, albite, anorthite	NO	NO
St1993; E4022	–	whitlockite	Cu + Mg, Al, Si, P, S, K, Ca, Fe, Sn	Bronze
St2206; E4385	–	calcite Mg, malachite, quartz	Sn + S, Ca, Cu + Mg, Al, Si, P, Cl, Ti, Fe, Ag, Pb	Pb bronze
St2208; E4387	–	NO	Cu, Ag, Sn + Mg, Al, Si, P, S, Cl, Ca, Fe	bronze
St33593; E5271	–	gypsum	Cu + S, Cl, Sn	bronze
St33594; E5272	–	calcite, quartz, albite, anorthite, gypsum?, portlandite?	Cu + Mg, Al, Si, P, S, Cl, K, Ca, Fe, Ni, Sn	bronze
St57210	–	calcite Mg, pyromorphite	Cu, Sn, Pb + Mg, Al, Si, P, Cl, K, Ca, Ti, Fe, As	Pb bronze
St57216	Paraloid	calcite Mg, albite, anorthite	Cu + Mg, Al, Si, P, Cl, Ca, Fe, Ni, As, Sn, Sb, Pb	Pb bronze
St57220	–	calcite Mg	Cu, Sn, Pb + Al, Si, P, Cl, Fe, As	Pb bronze
St57244	–	quartz, azurite, malachite, cerussite	NO	NO
St57250	–	calcite Mg, azurite, cuprite	Cu + Mg, Al, Si, P, S, Cl, Ca, Fe, Sn, Pb	Pb bronze
St57262	–	calcite Mg, cerussite, malachite, azurite, quartz, pyromorphite	Pb + Cu, Sn + Mg, Al, Si, P, S, Cl, Ca, Fe	Pb bronze
St114083; E5384	–	NO	no results	NO
St114084; E5385	–	NO	Cu, Sn + Mg, Al, Si, P, S, Ca, Pb	Pb bronze
St124133; E4537	–	Carbonate hydroxyapatite	NO	NO
St124142; E4491	–	calcite, quartz, albite, anorthite	Cu + Mg, Al, Si, P, K, Ca, Fe	copper
St139651; E4932	–	calcite, malachite, quartz, albite, anorthite	Cu, Sn + Mg, Al, Si,P, K, Fe, As, Pb	Pb bronze
St139652; E4933	–	malachite, quartz	Cu + Mg, Al, Si, P, K, Ca, Mn, Fe	copper?
E5552	malachite	quartz, dolomite	Cu, Pb, Sn, As + Al, Si, P, S, Cl, Fe, Ag	Pb bronze
E5553	malachite	quartz, cerussite, malachite	Cu, Pb, Si + Mg, Al, P, S, K, Ca, Fe, Sn	Pb bronze

(*continued on next page*)

Table 4 (*continued*)

Inv. no.	μ-Raman	μ-XRD	SEM-EDS	Interpr.
E5667	–	quartz, albite, anorthite, dolomite	Cu, Sn, Pb + Mg, Al, Si, S, K, Ca, Fe, As	Pb bronze
E5865	–	NO	Cu + Na, Mg, Al, Si, P, S, Cl, K, Ca, Ti, Fe, As, Sn, Pb	Pb bronze
E5868	–	calcite Mg, quartz	Cu, Sn, Pb + Mg, Al, Si, P, S, Cl, K, Ca, Fe, As	Pb bronze
E5873	–	–	Pb, Cu, Sn + Al, Si, P, Cl, Ca, Fe	Pb bronze
E5957	–	calcite Mg, albite, anorthite, teallite, silver?, mckinstryte?	Bronze bead (Cu + Mg, Al, Si, P, S, Cl, Ca, Fe) & silver (Ag + S + Mg, Al, Si, Cl, Ca, Fe, Cu)	copper/ bronze/ silver?
E5958	–	calcite Mg, albite, anorthite, teallite?	Bronze bead (Pb, Cu + Mg, Al, Si, P, Cl, K, Ca, Fe) & silver (Ag + S + Mg, Al, Si, Cl, Ca, Fe, Cu)	copper/ bronze/ silver?
E13225	cerussite	quartz, cerussite	Cu, Sn, Pb + Al, Si, S, Ca, As	Pb bronze
E13273	–	calcite, teallite? albite, anorthite, quartz	Cu, Sn + Al, Si, P, S, Cl, Ca, Ni, As, Ag	Bronze
E17738	–	quartz, albite, anorthite, cuprite	Cu, Sn, Pb + Mg, Al, Si, P, Fe, As	Pb bronze
D1660	–	calcite, cassiterite, malachite	Cu + Mg, Al, SI, P, S, Cl, K, Ca, Fe	Bronze
D1667	–	NO	NO	NO
D1668	–	calcite, anorthite, albite	Cu, Si + Mg, Al, S, Cl, K, Ca	copper?
D1669	–	calcite, quartz, albite, anorthite	NO	NO
D1750	–	calcite Mg, quartz	Cu + Al, SI, S, Ca	copper?
D2049	–	calcite, albite, anorthite, malachite, cassiterite, tenorite, teallite, tennantite	Cu, Sn, Pb + Mg, Al, Si, P, S, Cl, K, Ca, Mn, Fe	Pb bronze
D2059	cerussite	calcite, cuprite, paratacamite, malachite, mcguinnessite?	Cu, Pb + Al, Si, P, S, Ca, Fe	Pb bronze
D2064	–	calcite, cassiterite, tenorite	Cu + Mg, Al, Si, P, S, Ca	Bronze?
D2065	–	gypsum	NO	NO
D2073	–	calcite, tennantite	Cu, Pb + Mg, Al, SI, P, Cl, Ca, Mn, Fe, Sn	Pb bronze
D2077	–	calcite Mg, albite, anorthite, teallite, butlerite?	body: Cu, Sn, Pb + Mg, Al, Si, P, S, Cl, K, Ca, Fe. Pin: Cu + Mg. Al, Si, P, S, Cl, K; Ca, Ti, Fe, Sn	Pb bronze
D2104	malachite	calcite, albite, anorthite	Cu, Sn, Pb, Si, S + Mg, Al, P, Cl, K, Ca, Fe	Pb bronze
D2773	–	malachite	Cu, Sn + Mg, Al, Si, S, Cl, K, As, Ag.	bronze

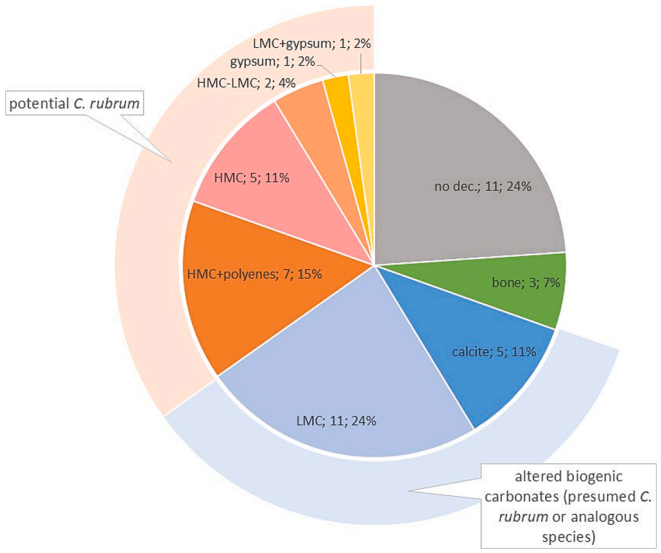

Fig. 3. Percentage composition of the whitish materials used to decorate the studied archaeological artefacts.

St33593 Longone pendant (7th century BCE: Fig. 2, # 46; Table 3; Fig. 7a-b-c) and the D2065 fibula remnants (Fig. 2, # 9; Table 3). In the former, gypsum is apparently the sole component; however, canalicular micro-morphologies relatable to coral are observed by OM (Fig. 7e), accounting for possible sulfation of an original carbonate. In the latter – in which combustion at high-T caused total bronze loss, leaving only the terracotta core – gypsum is detected by μ-Raman together with anhydrite ($CaSO_4$: bands at ≈ 1137, 1014 and 497 cm^{-1}) and LMC (average Mg-content by EDS: 6.89, ranging between 4.63 and 9.15 $MgCO_3$ mol %).

Carbonate-hydroxyapatite and whitlockite (phosphates found in skeletal bones and calcified tissues/bones, respectively: Lagier and Baud, 2003) are identified by μ-XRD in 3 artefacts (D1667 and St1993/124133; Table 3; Fig. 2, # 8, 35 and 36). Though previously reported as coral (Roncoroni, 2005), a bone nature is instead suggested here, as supported by μ-Raman (apatite band at ≈ 961 cm^{-1}) and EDS (abundant P and Ca). Besides, bone morphologies are also observed at the optical microscope (e.g., mosaic morphology, surface cracking and inner microporosity; Fig. 8; Pokines et al., 2018; Tappen and Peske, 1970). D1667 and St124133, due to their colouring and deformation, are possibly burnt bone remains (Gonçalves et al., 2011; Krap et al., 2017). St1993 is the older composite bow fibula of the set (675–600 BCE).

3.1.3. *Lack of decorating materials*

In 11 artefacts (St864/865/2208/139652; E5552/5553/5667/5865/5873/17738; D2773; Fig. 2, # 43, 44, 17, 22, 28, 26, 25, 27, 20, 14 and 2: ten *sanguisuga* fibulae with circular/occhio di dado decoration and one Valvaraita fibula with occhio di dado decoration, unburnt), μ-XRD detects only soil residues (e.g., quartz, feldspars) and bronze alteration byproducts (Table 3).

3.2. *Metal alloy*

A bronze alloy is mostly identified on the artefacts surface, systematically affected by serious degradation issues. μ-XRD and SEM-EDS detect Cu, Sn and eventually Pb-phases (i.e., malachite/azurite; cuprite, tenorite, tennantite and paratacamite, cassiterite, cerussite, teallite and pyromorphite). μ-Raman usually yields no appreciable signals, due to fluorescence (Table 4).

A composition akin to pure bronze (Cu and Sn: Table 4) is found in 12 artefacts of different kinds (*sanguisuga* and composite bow fibulae, Longone pendant and grooming tool, mostly unburnt: St864/1230/

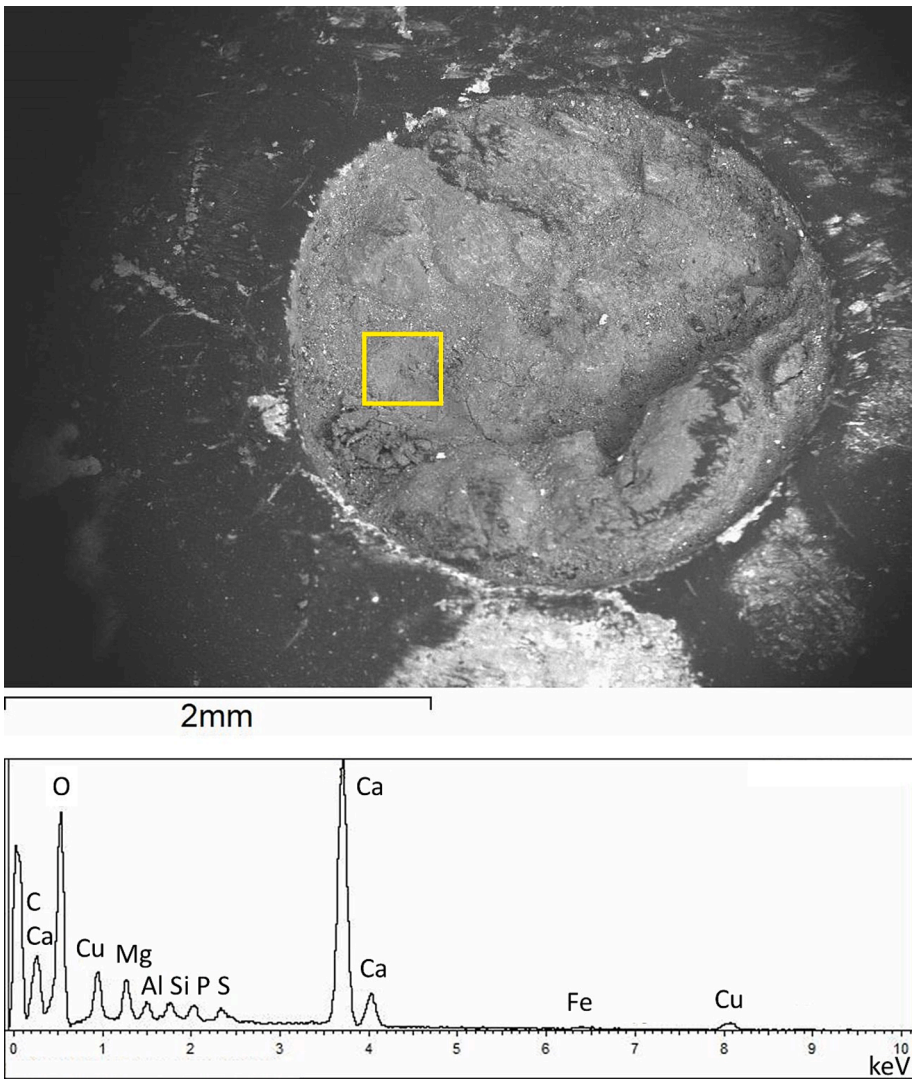

Fig. 4. St57216 artefact: (a) BSE-image of a circular decoration; (b) chemical analyses performed by EDS in the yellow square area. (For interpretation of the references to colour in this figure legend, the reader is referred to the web version of this article.)

1993/2208/33593/33594; E5957/5958/13273; D1660/2064/2773: Fig. 2, # 43, 40, 35, 17, 46, 45, 41, 42, 38, 11, 12 and 2). Two of them (E5957 and 5958: composite bow fibulae) also contain traces of Ag sulphide, detected on small blackish rods, purposely applied as decorative items upon small HMC beads (Fig. 9).

A lead-bronze composition (with subordinate Pb and related byproducts) is found in 23 artefacts (St865/879/2206/572https://doi.org/10/57216/57220/57250/57262/114084/139651; E5552/5553/5667/5865/ 5868/5873/13225/17738; D2049/2059/2073/2077/2104: Fig. 2, # 44, 23, 18, 31, 29, 30, 34, 33, 15, 21, 28, 26, 25, 27, 24, 20, 19, 14, 10, 13, 1, 3 and 5 – mostly *sanguisuga* fibulae, all unburnt except D2073). Though the measured average percentage values of Pb (as well as those of Cu and Sn) are inevitably biased by segregation or enrichment phenomena from production or post-depositional processes (being hardly accountable for the original alloy composition), its abundance suggests that such an addition may be intentional (3 % limit for alloy composition analysis) (Giumlia-Mair, 1998). In two cases (D2077 and St879), compositional differences exist between the body (bow and foot) and the pin of the fibula – with lead appearing only in the former.

In 4 cases (St124142/139652; D1668/1750: Fig. 2, # 39, 22, 7 and 4; 3 Longone pendants and 1 *sanguisuga* fibula, all unburnt), only Cu is detected.

The 7 residual artefacts provide no interpretable data (in 3, metal is not even conserved).

4. Discussion

4.1. Decorating materials

The mostly carbonatic nature of these decorations, coupled to other instances about their (more or less detailed) morphology, chronology and context of retrieval, brings to interesting considerations.

Obviously, the decorations of the seven specimens in which both high-Mg-calcite and polyenes are found (all extended foot *sanguisuga* fibulae with circular decorations insets) – often coupled to the observation of typical micro-morphologies – consist of *C. rubrum*. This dual detection seems to rely on the specific conditions of retrieval – i.e., inside a crucible, datable to 475–410 BCE (in excavations pertaining to the 20th century CE; older one: 1920, for the E13225 fibula foot; Fig. 2, # 19; more recent one: 1981/1985, for the fibulae from Via Isonzo). This confined context may have protected these materials from (more or less severe) external environmental issues, which might have caused their transformations and/or decay preventing a sharp identification. Despite their certain attribution to red coral, these decorations methodically show a white hue (Fig. 2). Probably, the chromophores of polyenes are

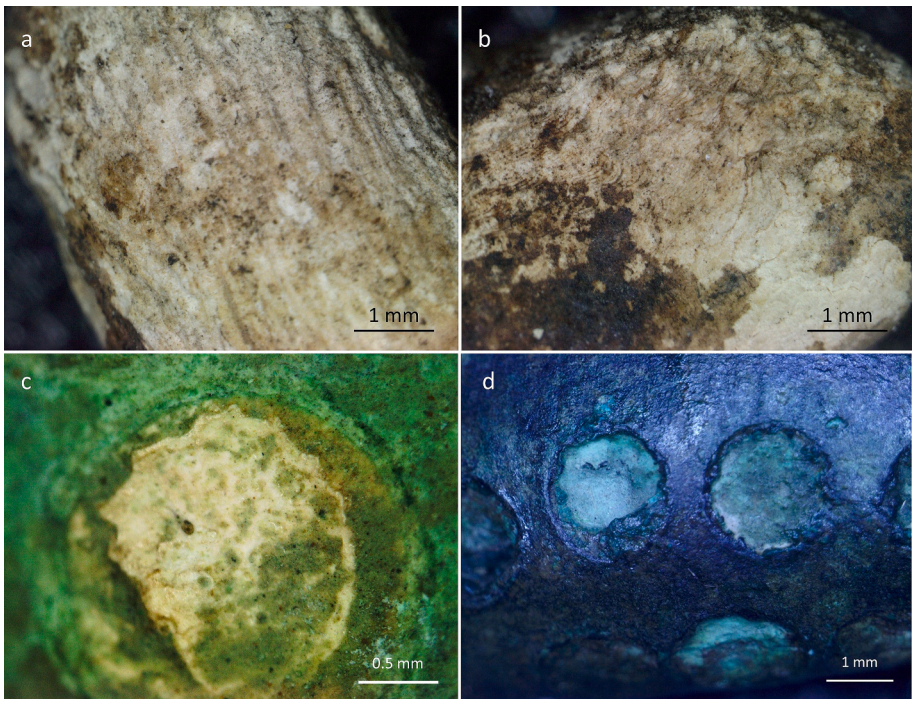

Fig. 5. OM-image of the surface of: a) D1750, longitudinal crenulations; b) D1750, growth rings; c) St57210, inset in the circular decoration, garland-like morphology; d) St2206, marked presence of metal alteration products.

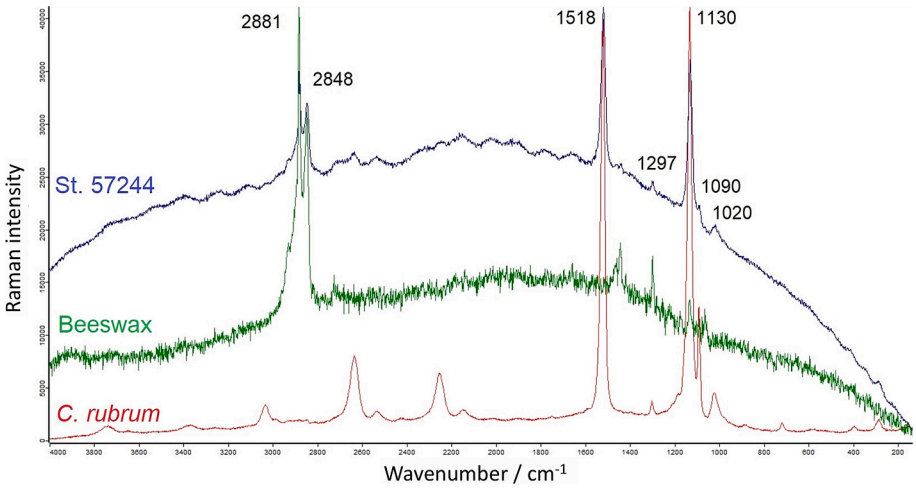

Fig. 6. Raman spectrum of the circular decoration in the St57244 artefact (blue); for comparison purposes, the spectra of beeswax (green) and Corallium rubrum (red) are also shown; 10X magnification, D0.3 filter. (For interpretation of the references to colour in this figure legend, the reader is referred to the web version of this article.)

likely to denaturate over time and/or under the action of (even slightly modified) environmental conditions. Nevertheless, conservation inside a crucible allowed the signature of their molecules to remain readable by Raman. The fact that these artefacts underwent no combustion (in spite of their context of retrieval – usually apt for this goal), further contributes to support this hypothesis. Moreover, by considering the limited time span to which this crucible is referred to (≈ 65 years), one might be tempted to assume that analogous decorating materials of biogenic nature (i.e., red coral) might also have been used for chronological purposes on other similar coeval artefacts. In the studied set, six other finds have a similar dating – 3 *sanguisuga* fibulae in which no filler is preserved (E5552/5553/5865; Fig. 2, # 28, 26 and 27) and 3 composite bow fibulae, two of which with HMC and one with LMC (E5957/5958; St1397; Fig. 2, # 41, 42 and 37). For the implications discussed below, it is reasonable to believe that *C. rubrum* might indeed have been used in some of these specimens too (lack of certainty depending on total loss of the decorating materials or denaturation of polyenes). Detection of beeswax, associated to coral, in the St57244 fibula (Fig. 2, # 32) may hint the use of a binder, in order to help adhesion to the hosting cavity. Yet, the Raman signatures of beeswax and synthetic wax are similar, and both materials were also used for restoration purposes in more recent times. Due to lack of historical record, the actual reason about presence of beeswax remains therefore unknown.

A biogenic origin for the decorating materials can also be certainly acknowledged for the other five artefacts in which HMC is detected with no polyenes. A high Mg-content, in fact, represents an undeniable clue leading to these carbonates biogenic nature (Vielzeuf et al., 2013; Fürst et al., 2016). Besides, in most of these finds the typical micro-

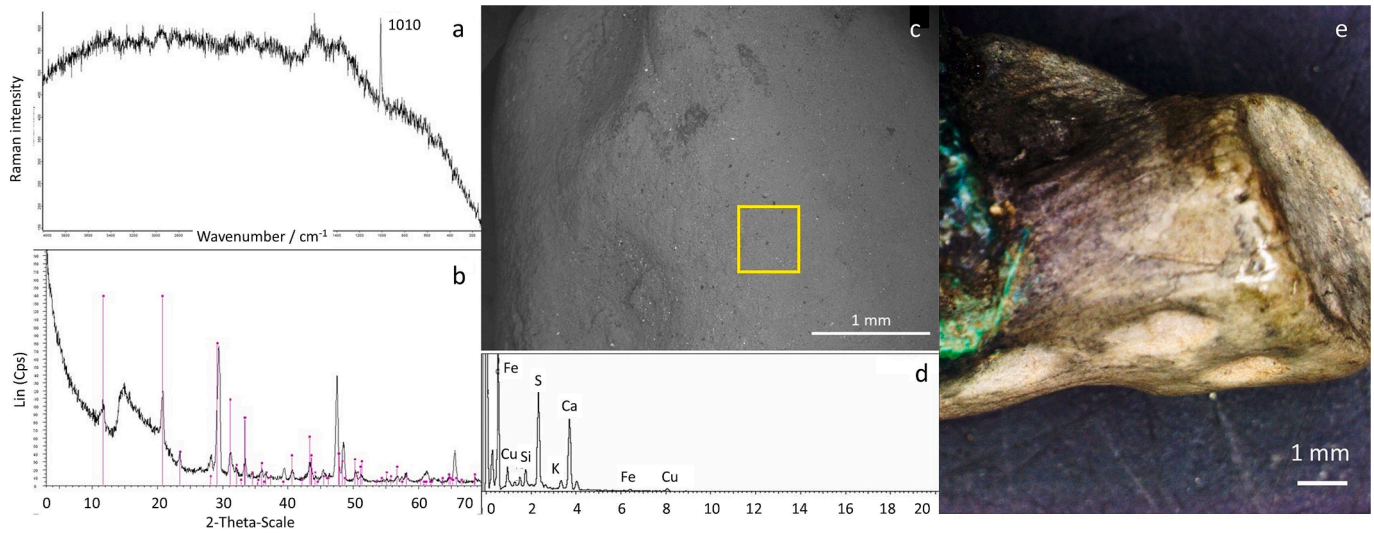

Fig. 7. St33593 artefact: a) μ-Raman spectra (20X magnification, D0.3 filter); the signal at 1010 cm^{-1} suggests presence of anhydrite; b) μ-XRD diffractogram; gypsum reflections in fuchsia); c) BSE-image (yellow square: site of EDS analysis); d) related EDS spectrum; e) OM-image of the surface with typical canalicular morphology. (For interpretation of the references to colour in this figure legend, the reader is referred to the web version of this article.)

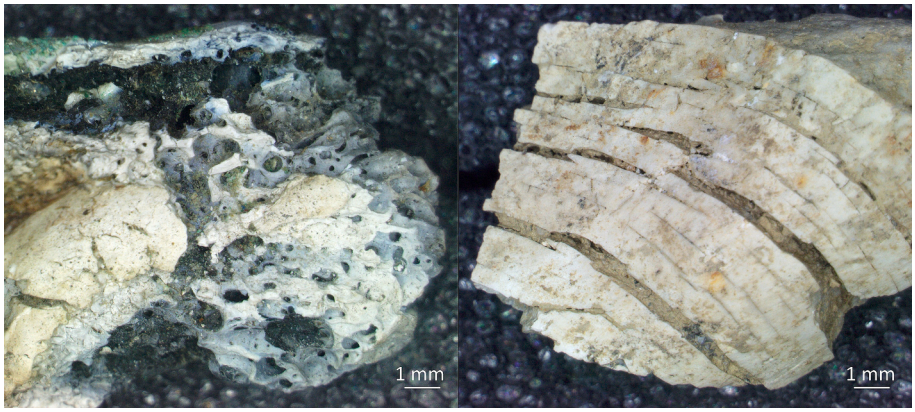

Fig. 8. OM-images of: (a) micro-porosity in D1667; (b) fractures and deformation in St124133.

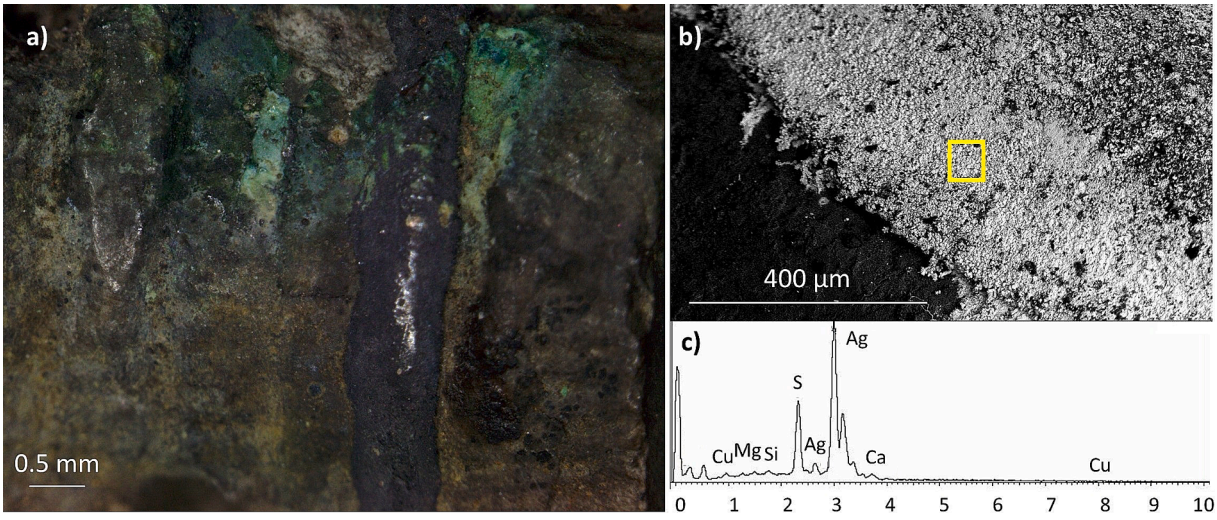

Fig. 9. OM-image of the silver rod on the HMC bead of the E5957 fibula: a) detail of the black band, in relief with respect to the surrounding areas; b) BSE-image of the black band (clearer in BSE image; the yellow square marks the analytical spot); c) related EDS spectrum. (For interpretation of the references to colour in this figure legend, the reader is referred to the web version of this article.)

morphologies of coral are clearly revealed by OM. Lack in detecting the Raman signature of polyenes might possibly be related, as hinted above, to an intervened denaturation and/or decay after environmental issues (e.g., endured during the artefacts interment before retrieval: e.g., soil composition, flowing of acid aqueous solutions, unusual temperature and/or humidity conditions: Fürst et al., 2016), or even to an unlikely (yet undetected) combustion of the artefacts. Use of red coral in these artefacts is thus almost certain, though the chance for other marine species (i.e., different corals or others) to also have been used cannot be completely ruled out. The current state of the art, in fact, prevents so far an extremely accurate phylogenetic attribution (Berruto et al., 2023).

An analogous biogenic origin can be postulated also for the two artefacts in which both HMC and LMC are found in different analytical spots of the same decorative inset. Conventionally, calcite with Mg $\geq$ 10.5 mol % $MgCO_3$ is defined as HMC, but a debate exists about the threshold that discriminates HMC from LMC. According to some authors, both LMC (0–5.5 mol % $MgCO_3$) and HMC (10.5–20 mol % $MgCO_3$) exist in nature, but unaltered calcites with intermediate values may not (Borromeo et al., 2017). HMC (even in *C. rubrum*) is metastable, as is aragonite forming the skeleton of other white corals (Angelini and Molin, 2015; Fürst et al., 2016; McGregor and Gagan, 2003). Due to this, the meteoric diagenesis of carbonates after environmental issues may cause a progressive and significant loss in the Mg-content of an original HMC, gradually transforming it into LMC *via* a selective Mg^{2+}/Ca^{2+} substitution. This phenomenon is not expected to necessarily affect homogeneously the whole decoration surface: different areas of a single specimen may have significantly variable Ca^{2+}/Mg^{2+} ratios, thus representing another hint of a possible biogenic origin (Floquet et al., 2015; Vielzeuf et al., 2013; Berruto et al., 2023). This hypothesis is further supported by the detailed observation, on these finds surfaces, of some (quite altered) micro-morphologies typical of *C. rubrum* (whose pigments, obviously, had decayed long ago due to bad conservation issues).

Sole presence, in the decorations, of either LMC (11 artefacts) or pure calcite (5) raises other interesting issues. To justify their detection, two alternative options might be considered (Berruto et al., 2023):

i. the occurrence, throughout the artefacts interment in the soil before modern retrieval, of alteration phenomena (analogous to those described above) that affected an original *C. rubrum*;
ii. the use, at the time when the artefacts were forged, of non-biogenic either sedimentary or metamorphic carbonate rocks (e.g., limestone or marble), or even others formed after consolidation of biogenic carbonate remnants (i.e., nummulite shells or fossil coral skeletons).

Interestingly, in the considered record all finds with decorations made of either LMC or pure calcite are older than those in which *C. rubrum* is certainly – or very likely – used (i.e., those already described above) – with a sole exception (St1397; Fig. 2, # 37). These artefacts, mostly of which unburnt, belong in fact to the GI or GII phase (Table 1). Apparently, this evidence might suggest that inorganic carbonate materials may have been used in different chronological periods or geographical contexts – in agreement with the second of the options listed above (a hypothesis at times advanced in the literature: Bente et al., 2015; Fürst et al., 2016; Gerdes et al., 2015; Schrickel and Bente, 2013). Nevertheless, such an option (i.e., resort to non-biogenic carbonate sources – rather than coral) appears questionable. Micro-morphologies ascribable to red coral are, in fact, clearly observable in most (7 out of 11) of the LMC-containing decorations (e.g., garland-like morphologies – Fig. 10a – in the D2049 *sanguisuga* fibula – Fig. 2, # 10; branch-morphologies and crenulations – Fig. 10.b – in the D1668 "Longone" pendant – Fig. 2, # 7) and seldom even in the pure-calcite ones (e.g., crenulations in the St33594 Longone pendant; Fig. 2, # 45). Besides, lack of coral micro-morphologies in LMC or pure-calcite decorations is not necessarily expected to discriminate the use of different (i.e., inorganic) carbonate materials. These distinguishing micro-shapes and features, in fact, are observable only on those decorations in which handcrafting did not require the biogenic materials (i.e., coral) to be excessively manipulated (e.g., in the "Longone al Segrino" pendants or in the composite arch-fibulae). Actually, these LMC and/or pure-calcite decorations are mounted on artefacts of various types – for some of which shaping, wedging and insertion in the hosting supports during manufacture may have required specific adjustments. This is the case, for example of the *sanguisuga* fibulae with insets, which hardly show coral micro-morphologies (with the exception of D2049) since the decorating materials had to undergo sophisticated manipulations (potentially altering these micro-features), useful to ensure their correct shaping and positioning. Furthermore, it has also been speculated in the literature that the manufacture of these decorations may also have involved a preliminary preparation of a coral-based paste, obtained by mixing ground coral powder with a binder, then spread in the hosting cavities and left to dry. When observed at the OM, these compacted coral powders hardly retain traces of their original micro-features, mostly obliterated by preliminary grinding (Berruto et al., 2023). As a result, when either LMC or pure calcite decorations are concerned (that is, in those cases where presence of micro-morphologies might represent a fundamental clue about the coral or non-coral nature of these materials), the detection of these micro-features might also rely on the peculiar kind and/or extent of the manufacturing process.

It has to be pointed out that these LMC decorations – similarly to others described above, in which both HMC and LMC are contextually present – show quite variable Mg contents, even within the same find. Besides supporting a potential biogenic origin (Floquet et al., 2015; Vielzeuf et al., 2013; Berruto et al., 2023), such an aspect brings an inevitable level of uncertainty as far as the exact Mg quantification is concerned. The total Mg wt.% content for a given artefact, in fact, is obtained by averaging the values of all EDS spot (or micro-area) analyses

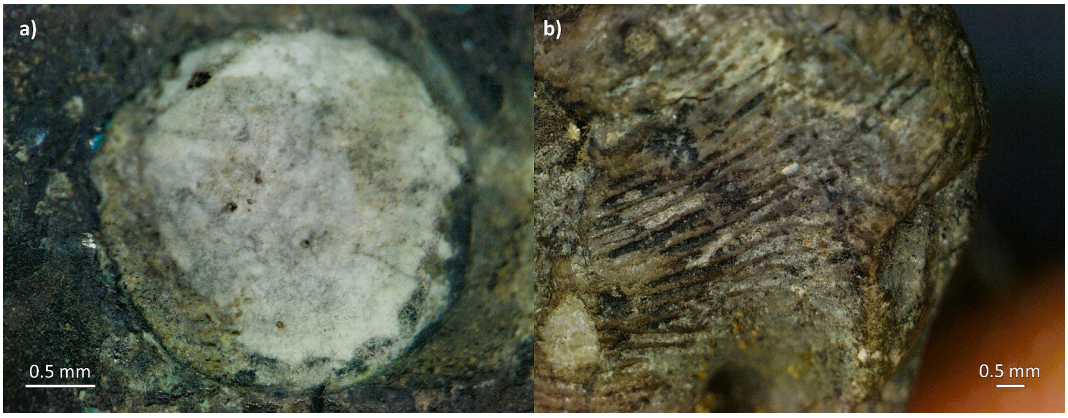

Fig. 10. OM-image of the surface of: a) D2049, garland-like morphology; b) D1668, crenulation or canalicular morphology.

– and assuming this dataset to be representative of the specimen. This assumption, however, has an implicit (albeit inevitable) degree of arbitrariness. Such a limitation, coupled to the (only) semi-quantitative valence of the EDS analyses (being performed on untreated samples), causes the discussed values to be taken *at least* cautiously. However, by weighing all pros and cons, these evidences and/or limitations seemingly suggest that these LMC and pure-calcite decorations (16 artefacts) are more willingly to be justified by post-depositional diagenesis processes affecting biogenic carbonates (e.g., during the artefacts burial) (Schrickel et al., 2013, 2014; Bente et al., 2015), rather than to the use of inorganic/abiotic materials from sedimentary or metamorphic rocks of analogous compositions (e.g., limestones or marbles). Obviously, the very same diagenetic processes were also responsible for the denaturation of the related (if any) pigments. However, the current state of the art – and especially the need for adopting a non-invasive analytical protocol, to safeguard these finds integrity – can offer so far no further detail about these carbonates origin and/or history (i.e., whether, at the time of manufacture, either 'fresh' corals were used – which underwent diagenesis during the artefacts interment – or rather more or less consolidated remnants of fossil coral skeletons).

Sporadic detection (in 2 artefacts) of gypsum raises the question whether its presence might be intentional or rather result from alteration phenomena. Transformation of $CaCO_3$ into gypsum after sulfation is a well-known process, with SO_2 and SO_4^{2-} representing sulphur sources in air and water (Charola et al., 2007; Siedel and Siegesmund, 2014). Its formation after weathering depends on several factors (e.g., pollutants concentration, moisture, surface heterogeneity and porosity), with a growth rate of few μm/year (Giustetto et al., 2020). Besides, this phenomenon is also known to happen in natural biologic environments under peculiar conditions: for example, in coralline calcifying algae (such as *Lithophyllum*, *Titanoderma* and *Phymatolithon*) the skeletal mineralogy can be altered from calcite (or calcite + aragonite) to gypsum (Van Driessche et al., 2019). Simulations were also performed on modern *C. rubrum*, proving that a superficial gypsum film can form when treated with a $(Na,NH_4)_2SO_4$ solution (Bente et al., 2015). Presence of LMC and gypsum in the D2065 *sanguisuga* fibula (Fig. 2, # 9) supports this hypothesis; besides, detection of anhydrite in the same artefact – possibly after dehydration of gypsum at high temperatures – confirms that a combustion indeed occurred (Deer et al., 1992; Kosztolanyi et al., 1987). Presence of gypsum in the St33593 pendant (Fig. 2, # 46) could also be traced to sulfation of a biogenic carbonate, after circulation of sulphate-bearing aqueous solutions in the soil (Ruiz-Agudo et al., 2016) possibly intervened during the artefact interment before retrieval. In this case, the observation of coral micro-morphologies at the optical microscope (Fig. 7e) accounts for pseudomorphism of gypsum after calcite – a phenomenon well known in nature (Vergès-Belmin, 1994; Ruiz-Agudo et al., 2015). This assumption is further reinforced by the fact that a similar pendant (St33594; Fig. 2, # 45) in the same necklace contains pure calcite.

Some of the studied composite bow and *sanguisuga* fibulae (e.g., E5957 and E5958, both with HMC decorations but no polyenes; Fig. 2, # 41 and 42) represent the most elaborate female *parures* ever found in the Golasecca culture. In these artefacts, detection of silver (by now altered in Ag-sulphide; Zumdahl and DeCoste, 2013) in the tiny rods applied as decorating motifs on the small HMC pearls has important archaeometric implications. Similar decorative rods have in fact already been described in the archaeological literature, but made of gold. For the first time they are found here in silver, as additional decorative items. Sophisticated skills and accuracy were thus requested for handcrafting these complex decorative patterns made of precious materials – presumably indicative of the wealth and social relevance of the addressees.

4.2. Metal alloy

Technological extrapolations about the composition of the metal alloy must be taken cautiously. Our data, in fact, provide only semi-quantitative analyses, mostly based on surface alteration byproducts, the chemistry of which is biased by processes occurred during interment (meteoric diagenesis) or post-excavation (e.g., cleaning, conservation, restoration, etc.).

All 23 artefacts in lead bronze are *sanguisuga*-shaped and navicella fibulae – i.e., complex artefacts with thin and articulated metal parts. In two cases (D2077 and St879; Fig. 2, # 3 and 23), the pins were analysed separately and proved to contain no lead. Such an evidence confirms that these artefacts should be considered as composite objects. Also, lead is never detected in the simpler artefacts (i.e., Longone al Segrino pendants). Addition of Pb is known to increase fluidity of the melt and lower the melting temperature, favouring casting work typical of the lost-wax technique. Such an addition, however, is deleterious for hammering, because it increases heterogeneity and weakens the alloy sturdiness (Giumlia-Mair, 1998, 2000, 2003). A precise technical choice probably regulated addition of lead, aimed at producing specific types of artefacts – or even specific parts within a single object, realised in different casting steps. Pb was probably added for the lost-wax production of the *sanguisuga* and navicella fibulae body, which require a higher fluidity while casting, but not for the pin of the same artefacts, which was produced separately by hammering (necessitating of higher strength and elasticity). In the same way, Pb was not added to the small rods of the composite bow fibulae and Longone pendants, also requiring hammering.

5. Conclusions

A multi-analytical and strictly non-invasive archaeometric protocol is proposed for studying the whitish insets of presumed red coral used as decorative items on Iron Age bronze fibulae, while totally safeguarding their integrity. 46 artefacts belonging to the Golasecca culture, mainly in bronze and adorned by decorative insets, were studied as a dataset. The decorating materials are often identified as carbonates; although this evidence is not sufficient, *per se*, to attribute them to red coral, other more detailed specifications may help in solving such an issue. The adopted procedure provided very interesting results, opening further perspectives.

In detail, μ-XRD, μ-Raman and SEM-EDS unequivocally allowed identifying presence of HMC + polyenes, sole HMC or a mixture of HMC + LMC in the decorations of several artefacts (7, 5 and 2, respectively). In these specimens, the distinctive micro-morphologies of coral are often observed at the OM. All these evidences (presence of pigments, relevant Mg^{2+} content and micro-morphologies) allow attributing a biogenic origin to these carbonates, relatable with all due probability to *C. rubrum* (though, in some cases, the chance for other marine species to be also involved cannot be totally ruled out). Incidental lack of polyenes may be explained by an intervened denaturation after environmental issues, during the artefacts burial before retrieval. However, even when present, these pigments chromophores are inevitably lost, bleaching these materials.

Also, in other artefacts the same protocol allowed identifying presence of sole LMC (11 artefacts) or pure-calcite (5) – with no polyenes. For these carbonates, partial or complete loss of Mg^{2+} from the crystal lattice (and consequent substitution with Ca^{2+}) could be justified by a more severe and prolonged meteoric diagenesis, presumably occurred during the artefacts interment (and responsible as well for pigments denaturation). This hypothesis is supported by the typical coral micro-morphologies being observed in most LMC-containing specimens (7 out of 11) (and seldom even in the pure-calcite containing ones), which show highly variable Mg-quantities in different areas of the insets. A biogenic origin for these decorating materials (i.e., from red coral) can thus certainly be acknowledged – in particular for those specimens where these micro-features are detected (their lack, leaving instead some doubts).

As far as detection of other decorative materials (i.e., different from carbonates) is concerned, presence of gypsum in 2 artefacts (alone or

coupled to LMC) is apparently the result – in both cases – of sulfation of biogenic carbonates after burial in acidic soils and pseudomorphism of gypsum after calcite (with or without residual presence of LMC). Both of these artefacts should then be counted among those whose decorations were originally made of biogenic carbonate (i.e., red coral or similar species). Differently, presence of Ca-phosphates in 3 artefacts, coupled to the observation of bone morphologies at the OM, must indeed be related to the use of different materials (i.e., bones).

Based on these premises, by following a restrictive interpretation (that is, for LMC and pure-calcite a biogenic origin is attested *only* when coral micro-morphologies are observed), we can state that *C. rubrum* (or a similar species) is certainly identified with a more than appreciable level of certainty in 24 out of the 46 studied artefacts. Nevertheless, it must be considered that the non-systematic detection of coral micro-morphologies might also depend on specific issues involving the manufacturing of these decorations (e.g., preliminary coral grinding and/or more or less sophisticate handcrafting), which may cause morphological variations responsible for their hiding/obliteration. Thus, according to an extensive interpretation (that is, all LMC and pure-calcite carbonate insets should have a biogenic nature), the number of artefacts whose decorations could have a biologic origin raises up to 32.

These numbers – by considering that 11 (out of 46) specimens conserved no appreciable traces of decorating materials (being potentially excludable from computation) – cause the amount of cases in which biogenic carbonates (i.e., red coral or similar species) are found as decorating materials to constitute ≈ 69 (restrictive) or 91 % (extensive interpretation) of the studied decoration-bringing artefacts.

As far as provenance of *C. rubrum* is concerned – either natural (i.e., directly fished, at the time in which the artefacts were forged, from some Mediterranean coastal areas and/or exchanged by trades) or from fossiliferous rocks (i.e., derived from the diagenesis of coral skeletons sediments) – the current state of the art unfortunately prevents attaining this kind of information. This limitation is also related to the non-destructivity of the adopted protocol, which of course prevents the extrapolation of more in depth information that other invasive approaches (e.g., study in thin section at the optical polarizing microscope and SEM-EDS, isotopic analyses, etc.) might instead achieve.

Other considerations are also worth mentioning. By merely basing on chronological issues, one might be tempted to acknowledge that polyenes tend to be preserved only in the more recent artefacts. Such a conclusion, however, may be overrated, as the conservation (and consequent Raman detection) of these pigments may be influenced by other factors too. Polyenes are detected only in 15 % of the studied finds, retrieved in a crucible dated to the GIIIA phase. This dating, however, refers to the time when the artefacts were placed in the crucible for remelting – and *not* to the actual time of their production. In fact, albeit sharing the same typology (i.e. *sanguisuga* fibula with terracotta core and circular decorations), these items have both simpler (possibly, the older ones: GIIB) and more complex shapes (e.g. Palestro type – datable to the GIIIA1 phase). Conservation of polyenes is thus to be related here to the particularly protected context of discovery.

Similarly, one may be tempted to conclude that pure-calcite or LMC could preferentially be found in the older artefacts (GI-GII phases; 700–480 BCE). For the reasons discussed above, although these materials could result from either the use of rock-forming carbonates (e.g., limestones or marbles) or analogous minerals of biogenic origin (i.e., either 'fresh' coral skeletons – *C. rubrum* or white coral/madrepore – or fossil corals subjected to post-depositional alteration processes), the latter hypothesis seems more plausible.

An intervened artefact combustion might also influence either presence or lack of some decorating materials. Sporadic episodes have been discussed in the studied dataset (e.g., denaturation of polyenes, gypsum transformation into anhydrite), but no systematic correlation can be sketched so far.

As far as the composition of the metal alloy is concerned, this is mostly made of bronze or lead-bronze, depending on precise technological choices. In some cases, the alloy composition varies even within different parts of the same artefact. Addition of Pb was done whenever necessary, in order to improve the fluidity and workability of the molten state. Presence of a silver ribbon (nowadays altered in AgS) is identified on some composite bow fibulae of the more evolved type. This represents a sort of exception for these artefacts, in which golden ribbons are generally reported instead (De Marinis, 2000).

CRediT authorship contribution statement

Giulia Berruto: Writing – review & editing, Writing – original draft, Methodology, Investigation, Data curation. **Eliano Diana:** Writing – review & editing, Validation, Supervision, Methodology, Formal analysis. **Roberto Giustetto:** Writing – review & editing, Validation, Supervision, Methodology, Formal analysis.

Declaration of competing interest

The authors declare that they have no known competing financial interests or personal relationships that could have appeared to influence the work reported in this paper.

Acknowledgements

The authors thank the Soprintendenza Archeologia Belle Arti e Paesaggio per le province di Como, Lecco, Monza Brianza, Pavia, Sondrio e Varese and the Municipality of Como for allowing the archaeometric investigation of the artefacts and publication of the results. Special thanks go to Barbara Grassi, Gianmarco Cossandi and Clelia Orsenigo for their precious support. Marica Venturino, Nadia Curetti and Emanuele Costa are thanked for their invaluable help and support during data collection.

Appendix A. Supplementary material

Supplementary data to this article can be found online at https://doi.org/10.1016/j.jasrep.2025.105131.

Data availability

Data will be made available on request.

References

Angelini, I., Molin, G., 2015. Gli intarsi delle fibule e dei pendenti natura dei materiali, in: Gangemi, G., Bassetti, M., Voltolini, D. (Eds.), Le Signore Dell'Alpago. La Necropoli Preromana Di "Pian de La Gnela". Pieve d'Alpago (Belluno). Canova Edizioni, Treviso, pp. 52-53.

Barnard, W., de Waal, D., 2006. Raman investigation of pigmentary molecules in the molluscan biogenic matrix. J. Raman Spectrosc. 37, 342–352. https://doi.org/10.1002/jrs.1461.

Bente, K., Koenig, A., Dehn, F., Krüger, P., Wirth, R., Hirsch, D., Münster, T., Berthold, C., 2015. Vergleichende computertomografische und elektronenmikroskopische Studien zu eisenzeitlicher Korallenzier. METALLA, Jahrestagung Archäometrie und Denkmalpflege 7.

Bergamonti, L., Bersani, D., Csermely, D., Lottici, P.P., 2011. The nature of the pigments in corals and pearls: a contribution from Raman spectroscopy. Spectrosc. Lett. 44, 453–458. https://doi.org/10.1080/00387010.2011.610399.

Bergamonti, L., Bersani, D., Mantovan, S., Lottici, P.P., 2013. Micro-Raman investigation of pigments and carbonate phases in corals and molluscan shells. Eur. J. Mineral. 25, 845–853. https://doi.org/10.1127/0935-1221/2013/0025-2318.

Berruto, G., Costa, E., Curetti, N., Diana, E., Giustetto, R., 2023. Archaeometric investigation of bronze Iron Age fibulae with nestled coral insets from three archaeological sites of the Piedmont region (Northwestern Italy). J. Archaeol. Sci. Rep. 51, 104119. https://doi.org/10.1016/j.jasrep.2023.104119.

Borrello, M., 2001. Vous avez dit "corail"? Annuaire de la Société Suisse de Préhistoire et d'Archéologie 84.

Borrello, M., Bosch, J., Mazzorin, J., Martín, A., Esteve, X., Gorgoglione, M., Mariéthoz, F., Nadal, J., Oms, F.X., 2012. Les parures néolithiques en corail (Corallium rubrum L.) d'Europe occidentale. Rivista Di Scienze Preistoriche LXII 67–82.

Borromeo, L., Zimmermann, U., Andò, S., Coletti, G., Bersani, D., Basso, D., Gentile, P., Schulz, B., Garzanti, E., 2017. Raman spectroscopy as a tool for magnesium estimation in Mg-calcite. J. Raman Spectrosc. 48, 983–992. https://doi.org/10.1002/jrs.5156.

Brambilla, L., Tommasini, M., Zerbi, G., Stradi, R., 2012. Raman spectroscopy of polyconjugated molecules with electronic and mechanical confinement: the spectrum of Corallium rubrum. J. Raman Spectrosc. 43, 1449–1458. https://doi.org/10.1002/jrs.4057.

Casini, S., 2018. Una didracma di Populonia dall'abitato del Golasecca III A di Prestino-via Isonzo (Como). Rassegna Di Archeologia 26 (26), 67–85.

Casini, S., 2022. I principali insediamenti della cultura di Golasecca: un quadro d'insieme. Rivista di scienze preistoriche LXXII, S2, Preistoria e Protostoria in Lombardia e Canton Ticino, 531–562.

Charola, A.E., Pühringer, J., Steiger, M., 2007. Gypsum: a review of its role in the deterioration of building materials. Environ. Geol. 52, 339–352.

Cicolani, V., 2017. Passeurs des Alpes. La culture de Golasecca entre Méditerranée et Europe continentale à l'âge du Fer. Hermann Éditeurs, Paris.

De Marinis, R.C., 1981. Il periodo Golasecca III A in Lombardia. Studi Archeologici I, 229–232.

De Marinis, R.C., 2000. Il corallo nella cultura di Golasecca. In: Morel, J.P., Rondi-Costanzo, C., Ugolini, D. (Eds.), Corallo Di Ieri Corallo Di Oggi (atti Del Convegno, Ravello, Villa Rufolo, 13-15 Dicembre 1996). Edipuglia, Bari, pp. 159–175.

Deer, W.A., Howie, R.A., Zussman, J., 1992. An Introduction to the Rock-Forming Minerals, (2nd ed.). Pearson Education, England, p. 614.

De Marinis, R.C., 1997. Il corallo nella Preistoria e Protostoria dell'Italia settentrionale, in: Ori Delle Alpi. Catalogo Della Mostra. Trento, Castello Del Buonconsiglio, 20 Giugno - 9 Novembre 1997, Quaderni Della Sezione Archeologica Castello Del Buonconsiglio. Monumenti e Collezioni Provinciali. Trento, pp. 153–160.

De Marinis, R.C., 2009a. La culture de Golasecca: une histoire de plusieurs siècles. Golasecca du commerce e des hommes à l'age du fer (VIII-V siècle av. J.C.) (C. Lorre and V. Cicolani) 39–44.

De Marinis, R.C., 2009b. Signes de pouvoir et de richesse à Golasecca: du monde des morts à celui des vivants. Golasecca du commerce e des hommes à l'age du fer (VIII-V siècle av. J.C.) (C. Lorre and V. Cicolani) 45–53.

De Marinis, R.C., Gambari, F.M., 2005. La cultura di Golasecca dal X agli inizi del VII secolo a.C.: cronologia relativa e correlazioni con altre aree culturali, in: MEDITERRANEA. Quaderni Annuali Dell'Istituto Di Studi Sulle Civiltà Italiche e Del Mediterraneo Antico. Presented at the Oriente e Occidente: Metodi e discipline a confronto. Riflessioni sulla cronologia dell'età del Ferro in Italia, Atti dell'Incontro di studi, Roma 2005, G. Bartoloni - F. Delpino Eds., pp. 197–225.

Faudino, V., Ferrero, L., Giaretti, M., Venturino Gambari, M., 2014. Celti e Liguri. Rapporti tra la cultura di Golasecca e la Liguria interna nella prima Età del Ferro, in: Actes Du XXXVIe Colloque International de l'AFEAF (Vérone, 17-20 Mai 2012), Les Celtes et Le Nord de l'Italie. Premier et Second Âges Du Fer (a Cura Di Barral Ph., Guillaumet J.-P., Rouillère-Lambert M.-J., Saracino M., Vitali, D.). pp. 17–20.

Fernandes, R.F., Maia, L.F., Couri, M.R., Costa, L.A.S., de Oliveira, L.F.C., 2015. Raman spectroscopy as a tool in differentiating conjugated polyenes from synthetic and natural sources. Spectrochim. Acta A Mol. Biomol. Spectrosc. 134, 434–441. https://doi.org/10.1016/j.saa.2014.06.022.

Floquet, N., Vielzeuf, D., Ferry, D., Ricolleau, A., Heresanu, V., Perrin, J., Laporte, D., Fitch, A.N., 2015. Thermally induced modifications and phase transformations of red coral Mg-calcite skeletons from infrared spectroscopy and high resolution synchrotron powder diffraction analyses. Cryst. Growth Des. 15, 3690–3706. https://doi.org/10.1021/acs.cgd.5b00291.

Fürst, S., Müller, K., Gianni, L., Paris, C., Bellot-Gurlet, L., Pare, C., Reiche, I., 2016. Raman Investigations to Identify Corallium rubrum in Iron Age Jewelry and Ornaments. Minerals 6, 56. https://doi.org/10.3390/min6020056.

Gerdes, A., Bente, K., Berthold, C., 2015. Sr-und B-isotopie zum korallendekor latene-und hallstatt zeitlicher fibeln und korrelierbare objecte. METALLA, Jahrestagung Archäometrie Und Denkmalpflege 7, 47–48.

Giumlia-Mair, A., 1998. Studi metallurgici sui bronzi della necropoli di S. Lucia-Most Na Soči. Aquileia Nostra 69, 29–136.

Giumlia-Mair, A., 2000. Bronze Technology in the Eastern subalpine region between Final Bronze Age and Early Iron Age. na.

Giumlia-Mair, A., 2003. Evoluzione tecnica e formale nella produzione di fibule e spilloni tra il IX e il IV sec. ac nell'area Alpino-Orientale. Fibulae dall'età del Bronzo all'alto medioevo (a cura di E. Formigli) 2003, 49–58.

Giustetto, R., Berruto, G., Diana, E., Costa, E., 2013. Decorated prehistoric pottery from Castello di Annone (Piedmont, Italy): archaeometric study and pilot comparison with coeval analogous finds. J. Archaeol. Sci. 40, 4249–4263. https://doi.org/10.1016/j.jas.2013.06.012.

Giustetto, R., Pastero, L., Aquilano, D., 2020. Potential effects of the shape of gypsum aggregates on the early sulfation of marble and travertine. J. Build. Eng. 32, 101794.

Gonçalves, D., Thompson, T.J.U., Cunha, E., 2011. Implications of heat-induced changes in bone on the interpretation of funerary behaviour and practice. J. Archaeol. Sci. 38, 1308–1313. https://doi.org/10.1016/j.jas.2011.01.006.

Hasegawa, H., Rahman, M.A., Luan, N.T., Maki, T., Iwasaki, N., 2012. Trace elements in Corallium spp. As indicators for origin and habitat. J. Exp. Mar. Biol. Ecol. 414, 1–5. https://doi.org/10.1016/j.jembe.2012.01.005.

Kaczorowska, B., Hacura, A., Kupka, T., Wrzalik, R., Talik, E., Pasterny, G., Matuszewska, A., 2003. Spectroscopic characterization of natural corals. Anal. Bioanal. Chem. 377, 1032–1037. https://doi.org/10.1007/s00216-003-2153-1.

Kiefert, L., Karampelas, S., 2011. Use of the Raman spectrometer in gemmological laboratories. Spectrochim. Acta A Mol. Biomol. Spectrosc. 80 (1), 119–124. https://doi.org/10.1016/j.saa.2011.03.004.

Kosztolanyi, C., Mullis, J., Weidmann, M., 1987. Measurements of the phase transformation temperature of gypsum-anhydrite, included in quartz, by microthermometry and Raman microprobe techniques. Chem. Geol. 61 (1–4), 19–28.

Krap, T., van de Goot, F.R.W., Oostra, R.-J., Duijst, W., Waters-Rist, A.L., 2017. Temperature estimations of heated bone: a questionnaire-based study of accuracy and precision of interpretation of bone colour by forensic and physical anthropologists. Leg. Med. 29, 22–28. https://doi.org/10.1016/j.legalmed.2017.08.001.

Kupka, T., Lin, H.M., Stobiński, L., Chen, C.-H., Liou, W.-J., Wrzalik, R., Flisak, Z., 2009. Experimental and theoretical studies on corals. I. Toward understanding the origin of color in precious red corals from Raman and IR spectroscopies and DFT calculations. J. Raman Spectrosc. 41, 651–658. https://doi.org/10.1002/jrs.2502.

Lafuente, B., Downs, R.T., Yang, H., Stone, N., 2015. 1. The power of databases: The RRUFF project, in: Highlights in Mineralogical Crystallography. De Gruyter (O), pp. 1-30. RRUFF™ Project Database http://rruff.info/.

Lagier, R., Baud, C.-A., 2003. Magnesium Whitlockite, a calcium phosphate crystal of special interest in pathology. Pathol. – Res. Practice 199 (5), 329–335. https://doi.org/10.1078/0344-0338-00425.

Macchia, M., Resta, V., Quarta, G., Calcagnile, L., 2016. Precious coral nondestructive characterization by Raman and XRF spectroscopy. X-ray Spectrometry 45, 281–287.

Maia, L.F., Fleury, B.G., Lages, B.G., Barbosa, J.P., Pinto, Â.C., Castro, H.V., de Oliveira, V.E., Edwards, H.G., de Oliveira, L.F., 2010. Identification of reddish pigments in octocorals by Raman spectroscopy. J. Raman Spectrosc. 42, 653–658. https://doi.org/10.1002/jrs.2758.

Mangani, C., 2016. Corallo al Monsorino? In: Grassi, B., Mangani, C. (Eds.), Nel Bosco Degli Antenati. La Necropoli Del Monsorino Di Golasecca (scavi 1985-86). All'Insegna del Giglio, Firenze, pp. 131–132.

McGregor, H.V., Gagan, M.K., 2003. Diagenesis and geochemistry of Porites corals from Papua New Guinea: implications for paleoclimate reconstruction. Geochim. Cosmochim. Acta 67, 2147–2156. https://doi.org/10.1016/S0016-7037(02)01050-5.

Peroni, R., Carancini, G.L., Coretti Irdi, P., Ponzi Bonomi, L., Rallo, A., Saronio Masolo, P., Serra Ridgway, F.R., 1975. Studi sulla cronologia delle civiltà di Este e Golasecca. Origines, Sansoni Editore, Firenze.

Perrin, F., 2000. L'origine de la mode du corail méditerranéen (Corallium rubrum L.) chez les peuples celtes: essai d'interprétation, in: Corallo Di Ieri Corallo Di Oggi, Atti Del Convegno, Ravello, Villa Rufolo, 13-15 Dicembre 1996, Morel J.P, Rondi-Costanzo C., Ugolini D. (a Cura Di). Edipuglia, Bari, pp. 193–203.

Pokines, J.T., Faillace, K., Berger, J., Pirtle, D., Sharpe, M., Curtis, A., Lombardi, K., Admans, J., 2018. The effects of repeated wet-dry cycles as a component of bone weathering. J. Archaeol. Sci. Rep. 17, 433–441. https://doi.org/10.1016/j.jasrep.2017.11.025.

Rahman, M.A., Oomori, T., Wörheide, G., 2011. Calcite formation in soft coral sclerites is determined by a single reactive extracellular protein. J. Biol. Chem. 286, 31638–31649. https://doi.org/10.1074/jbc.M109.070185.

Roncoroni, F., 2005. La Cultura di Golasecca nella Collezione Garovaglio: l'area occidentale. AIS - Archeologia dell'Italia Settentrionale, Musei Civici di Como, Como.

Ruiz-Agudo, E., Álvarez-Lloret, P., Ibañez-Velasco, A., Ortega-Huertas, M., 2016. Crystallographic control in the replacement of calcite by calcium sulfates. Cryst. Growth Des. 16, 4950–4959.

Ruiz-Agudo, E., Putnis, C.V., Hövelmann, J., Álvarez-Lloret, P., Ibañez-Velasco, A., Putnis, A., 2015. Experimental study of the replacement of calcite by calcium sulphates. Geochim. Cosmochim. Acta 156, 75–93.

Schrickel, M., Bente, K., 2013. Bedeutung und Bedeutungsverlust roter Korallen: Archäologische und aturwissenschaftliche Studien zu eisenzeitlichen Fibeln., In: H. Meller u.a. (Hrsg.), Rot - Die Archäologie Bekennt Farbe. 5. Mitteldt. Archäologentag. Tagungen Landesmus. Vorgesch. 10 (Halle/S. 2013). pp. 341–352.

Schrickel, M., Bente, K., Berthold, C., Grill, W., Teschner, U., Sarge, C., Hoppe, T., 2014. Vergleichende archaometrische untesuchungen an mitteldeuschen korallenfibeln. Fragestellungen und methodischer uberblick. Universitätsforschungen Zur Prähistorischen Archäologie Band Aus Dem Institut Für Vor- Und Frühgeschichte Der Universität Mainz 258, 67–91.

Schrickel, M., Bente, K., Fleischer, F., Franz, A., 2013. Importation ou imitation du corail à la fin de l'âge du Fer? Première approche par analyses du matériau, In: Supplement Aquitania 30 (Pessac 2013). Presented at the L'âge du Fer en Aquitaine et Sur Ses Marges. Mobilité des Hommes, Diffusion des Idées, Circulation des Biens dans L'espace Européen à L'âge du Fer, Actes du 35e Colloque International de l'AFEAF, Bordeaux, 2011, pp. 753-759.

Schvoerer, M., Bechtel, F., N'Guyen, P.H., Clastre, J., Villeneuve, G., 2000. Repères afin de caractériser ou dater les coraux anciens, in: Morel, J.P., Rondi-Costanzo, C., Ugolini, D. (Eds.), Corallo Di Ieri Corallo Di Oggi (Atti del Convegno, Ravello, Villa Rufolo, 13-15 Dicembre 1996), Edipuglia, Bari, pp. 225-235.viollier.

Siedel, H., Siegesmund, S., 2014. Characterization of stone deterioration on buildings (Chapter 6). In: Siegesmund, S., Snethlage, R. (Eds.), Stone in Architecture. Springer-Verlag, Berlin Heidelberg, pp. 349–414.

Skeates, R., 1993. Mediterranean coral: its use and exchange in and around the alpine region during the later Neolithic and copper age. Oxf. J. Archaeol. 12, 281–292.

Smith, C.P., McClure, S.F., Eaton-Magaña, S., Kondo, D.M., 2007. Pink-to-red coral: a guide to determining origin of color. Gems Gemol. 43, 4–15.

Tagliente, M., 2006. Coralli segreti. Immagini e miti dal mare tra Oriente ed Occidente, In: Coralli Segreti. Immagini e Miti Dal Mare Tra Oriente e Occidente. Potenza, Museo Archeologico Nazionale Della Basilicata "Dinu Adamesteanu." pp. 11–19.

Tappen, N.C., Peske, G.R., 1970. Weathering cracks and split-line patterns in archaeological bone. Am. Antiq. 35, 383–386. https://doi.org/10.2307/278350.

Ugolini, D., 2006. Il corallo tra il VII e il II sec. a.C. lungo le coste della Catalogna e della Gallia, In: Coralli Segreti. Immagini e Miti Dal Mare Tra Oriente e Occidente. Potenza, Museo Archeologico Nazionale Della Basilicata "Dinu Adamesteanu." pp. 78–87.

Van Driessche, A.E.S., Stawski, T.M., Kellermeier, M., 2019. Calcium sulfate precipitation pathways in natural and engineered environments. Chem. Geol. 530, 119274.

Vergès-Belmin, V., 1994. Pseudomorphism of gypsum after calcite, a new textural feature accounting for the marble sulphation mechanism. Atmos. Environ. 28 (2), 295–304.

Vielzeuf, D., Garrabou, J., Baronnet, A., Grauby, O., Marschal, C., 2008. Nano to macroscale biomineral architecture of red coral (Corallium rubrum). Am. Mineral. 93, 1799–1815. https://doi.org/10.2138/am.2008.2923.

Vielzeuf, D., Garrabou, J., Gagnon, A., Ricolleau, A., Adkins, J., Günther, D., Hametner, K., Devidal, J.-L., Reusser, E., Perrin, J., 2013. Distribution of sulphur and magnesium in the red coral. Chem. Geol. 355, 13–27. https://doi.org/10.1016/j.chemgeo.2013.07.008.

Zumdahl, S.S., DeCoste, D.J., 2013. Chemical Principles, (7th ed.). Cengage Learning, p. 505.

Von Eles Masi, P., 1986. Le fibule dell'Italia settentrionale. Prähistorische bronzefunde XIV, 5. CH Beck, Munchen.